Synthesis of Ni-Based Metal-Organic Frameworks Using Five Distinct Precursors and Their Energy Storage Performance as Electrodes in Supercapacitor

By

Syeda Hamna Sakhawat

(Registration No: 00000403122)

Department of Energy Systems Engineering

US-Pakistan Centre for Advanced Studies in Energy (USPCAS-E)

National University of Sciences & Technology (NUST)

Islamabad, Pakistan

(2024)

Synthesis of Ni-Based Metal-Organic Frameworks Using Five Distinct Precursors and Their Energy Storage Performance as Electrodes in Supercapacitor

By

Syeda Hamna Sakhawat

(Registration No: 00000403122)

A thesis submitted to the National University of Sciences and Technology, Islamabad,

in partial fulfillment of the requirements for the degree of

Master of Science in

Energy Systems Engineering

Supervisor: Ghulam Ali

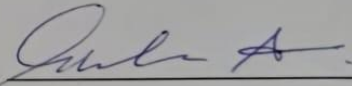US-Pakistan Centre for Advanced Studies in Energy (USPCAS-E)

National University of Sciences & Technology (NUST)

Islamabad, Pakistan

(2024)

THESIS ACCEPTANCE CERTIFICATE

Certified that the final copy of MS Thesis written by Ms Syeda Hamna Sakhawat (Registration No. 00000403122), of ESE, USPCASE has been vetted by the undersigned, found complete in all respects as per NUST Statutes/ Regulations/ Masters Policy, is free of plagiarism, errors, and mistakes and is accepted as partial fulfilment for the award of master's degree. It is further certified that necessary amendments as pointed out by GEC members and foreign/ local evaluators of the scholar have also been incorporated in the said thesis.
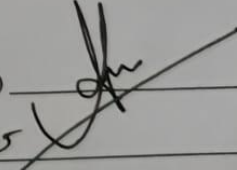
Signature: _____

Name of Supervisor _Dr. Ghulam Ali_

Date: _08—01—2025_

Signature (HOD): _____

Date: _09—01—2025_

Signature (Dean/ Principal) _____

Date: _14/01/2025_

National University of Sciences & Technology
MASTER'S THESIS WORK

We hereby recommend that the dissertation prepared under our supervision by Syeda Hamna Sakhawat (00000403122)

Titled: **Synthesis of Ni-based metal-organic frameworks using five distinct precursors and their energy storage performance as electrodes in supercapacitor**

be accepted in partial fulfillment of the requirements for the award of **MS Energy Systems Engineering** degree with (_____A_____) grade.

Examination Committee Members

1. Name: Prof.Dr Naseem Iqbal   Signature: _____

2. Name: Dr. Mustafa Anwar   Signature: _____

3. Name: Dr. Sehar Shakir   Signature: _____

Supervisor's name: Dr. Ghulam Ali   Signature: _____

Date: 06-12-2024

Prof.Dr Naseem Iqbal
Head of Department   Signature   Date 09-01-2025

COUNTERSIGNED

Date: 14/01/2025   Dean/Principal

US-Pakistan Center for Advanced Studies in Energy (USPCASE)

CERTIFICATE OF APPROVAL

This is to certify that the research work presented in this thesis, entitled "Synthesis of Ni-based metal-organic frameworks using five distinct precursors and their energy storage performance as electrodes in supercapacitor" was conducted by Ms Syeda Hamna Sakhawat under the supervision of Dr. Ghulam Ali. No part of this thesis has been submitted anywhere else for any other degree. This thesis is submitted to the US-Pakistan Centre for Advanced Studies in Energy (USPCASE) in partial fulfilment of the requirements for the degree of Master of Science in the Field of Energy Systems Engineering Department of USPCASE National University of Sciences and Technology, Islamabad.

Student Name: Hamna Sakhawat   Signature: _____

Examination Committee:
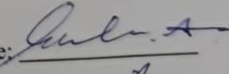
a) GEC Member 1: Dr. Naseem Iqbal   Signature: _____

      (Professor, ESE, USPCAS-E)

b) GEC Member 2: Dr. Sehar Shakir   Signature: _____

      (Assistant Professor, ESE, USPCAS-E)

c) GEC Member 3: Dr. Mustafa Anwar   Signature: _____

      (Assistant Professor, ESE, USPCAS-E)

Supervisor Name: Dr. Ghulam Ali   Signature: _____

Name of HOD: Dr. Naseem Iqbal   Signature: _____

Name of Principal/Dean: Dr. Adeel Waqas   Signature: _____

AUTHOR'S DECLARATION

I Syeda Hamna Sakhawat hereby state that my MS thesis titled "Synthesis of Ni-based metal-organic frameworks using five distinct precursors and their energy storage performance as electrodes in supercapacitor" is my work and has not been submitted previously by me for taking any degree from the National University of Sciences and Technology, Islamabad or anywhere else in the country/ world.

At any time if my statement is found to be incorrect even after I graduate, the university has the right to withdraw my MS degree.

Name of Student: ____Syeda Hamna Sakhawat____

Date: _____08-01-2025_____

PLAGIARISM UNDERTAKING

I solemnly declare that the research work presented in the thesis titled "Synthesis of Ni-based metal-organic frameworks using five distinct precursors and their energy storage performance as electrodes in supercapacitor" is solely my research work with no significant contribution from any other person. Small contribution/ help wherever taken has been duly acknowledged and that complete thesis has been written by me.

I understand the zero-tolerance policy of the HEC and the National University of Sciences and Technology (NUST), Islamabad towards plagiarism. Therefore, I as an author of the above-titled thesis declare that no portion of my thesis has been plagiarized and any material used as reference is properly referred/cited.

I undertake that if I am found guilty of any formal plagiarism in the above-titled thesis even after the award of MS degree, the University reserves the right to withdraw/revoke my MS degree and that HEC and NUST, Islamabad have the right to publish my name on the HEC/University website on which names of students are placed who submitted plagiarized thesis.

Student Signature: _____

Name: _____ Syeda Hamna Sakhawat _____

DEDICATION

Dedicated to my Beloved Parents"

ACKNOWLEDGEMENTS

TABLE OF CONTENTS

LIST OF TABLES

LIST OF FIGURES

LIST OF SYMBOLS, ABBREVIATIONS AND ACRONYMS

BET   Brunauer-Emmet-Teller

CV   Cyclic Voltammetry

ECSA   Electrochemically Active Surface Area

EDLC   Electric Double Layer Capacitor

EIS   Electrochemical Impedance Spectroscopy

FTIR   Fourier Transform Infrared Spectroscopy

GCD   Galvanostatic Charge Discharge

PM   1,10-phenanthroline monohydrate

BDC   Benzene-1,4-dicarboxylic acid

MEIM   2-Methylimidazole

BTC   Benzene-1,3,5-tricarboxylic acid

PEG   Polyethylene glycol

DMF   N, N Dimethylformamide

SEM   Scanning Electron Microscopy

XRD   X-Ray Diffraction analysis

XPS   X-Ray Photoelectron Spectroscopy

TEM   Transmission Electron Microscopy

ABSTRACT

For supercapacitor applications Metal organic framework as an electrode material have emerged as an attractive alternative for large scale energy storage due to their enormous specific surface area and porous structure. The crucial aspect is the selection of electrode material. Nickle has drawn a lot of attention because of its advantageous qualities, which include strong electrical conductivity, chemical stability, tunable oxidation states, and an overall contribution to the material's porosity and surface area. Herein, five distinct Ni-MOFs were synthesized through solvothermal methods using five distinct ligands to investigate their properties as supercapacitor electrode materials. The Brunauer-Emmett-Teller method is used to compute the specific surface area and Ni-PM MOF shows the highest surface area value among all prepared electrodes, calculated as 24.38 m^2g^{-1}. Ni-PM MOF has the highest specific capacitance of 1497 F g^{-1} at 0.5 A g^{-1} and charge transfer resistance Rct value of 0.82 Ω in comparison to all other prepared electrodes. Furthermore, demonstrating outstanding cycling stability of 94.1 % capacitance retention (5000 cycles). Results indicate that Ni-PM MOF, out of all the prepared Ni-MOFs, can provide the best performance demonstrated by all characterizations including XRD, SEM, TEM, XPS, BET, Raman and Electrochemical measurements as well. Overall, Ni-PM MOF can be used as a potential electrode material for a supercapacitor application due to better electrochemical performance compared to other Ni-MOFs.

Keywords: *Metal-organic frameworks; Supercapacitor; Ni-MOFs; Surface   area; Capacitance*

CHAPTER 1:   INTRODUCTION

1.1 Background

Although energy is essential to human development, the global economy and ecology have been severely impacted by the steady depletion of natural resources and the huge consequences of the greenhouse effect. It is important to consider how to ensure sustainable social and economic development considering the steadily declining ecological environment. An increasing number of people are becoming interested in some renewable energy sources, such as wind, solar, and tidal energy [1]. However, because they are typically influenced by the season, region, and environment, these renewable energy sources are frequently quite uncertain and unstable. The development of effective, reliable, and ecologically friendly energy storage and conversion technologies should be encouraged to maximize the usage of renewable energy sources. Researchers are trying to create storage devices with high energy conversion to address the ever-increasing need for inexpensive, clean energy [2]. In recent decades for more efficient energy storage devices like batteries and capacitors a substantial amount of effort has been made and there has been a symbolic upsurge in interest in adorning new technology. However, the low energy density of traditional capacitors and the poor power density of batteries have hampered their application in high-handed technologies, which gave rise to the concept of supercapacitors [3]. Academia and Researchers in industry have been fascinated by remarkable stability and efficiency exhibited by energy conversion and storage devices. Consequently, significant challenges in the design and development of these systems continue to be faced.

SCs (Supercapacitors) are environmentally friendly energy storage devices with a high-power density and extended cycle life. They do, however, have a comparatively low energy density. Increasing their capacitance and improving their capacities are necessary to improve their energy density [4]. Because of their high-power density, supercapacitors are employed in portable electronics and vehicles that run on them. Based on how they store charge, they can be divided into two primary categories: electrochemical double-layer

capacitors (EDLCs) and pseudo capacitors. Whereas EDLCs use electrostatic processes to store charge, pseudo capacitors use electrochemical reactions. The electrolyte's function in these devices is essential to their functionality [5], [6].

Researchers' interest in metal-organic frameworks (MOFs) has grown recently because of their potential to form a variety of controlled porous structures, high specific surface area, large number of active metal centers and good thermal stability which demonstrates superior capacitance when utilized with the SCs electrode materials. MOFs are highly organized crystalline solids formed through coordination of metal ions or metal clusters self-assembling with organic ligands. MOFs' high porosity and tunable pore sizes have made them popular in a change of domains, together with ion exchange [7], chemical sensing [8], gas storage and separation [9] , catalysis [10] , and other applications. Furthermore, advantaging from their rich porous structure and sizable specific area which increase interaction with the electrolyte and reveal more redox active sites, MOFs can be utilized as ions to take part in the Faraday reaction or as excellent electrode and have an extensive range of potential use in energy storage materials [11].

Global attention has been drawn to MOF, which is well known for its many metals' ion core and organic ligand combinations. MOF has undergone more than a thousand modifications since the first experimental report on the MOF structure, which concentrated on copper or cobalt metal. By replacing the metal core with different first-row transition metals such as Zn, Cd, Ni, Ni, Fe, Mg, Ca, Sr, or Ba, the subsequent MOFs have shown that the structure can be manufactured easily and can provide new features and capabilities. Bimetallic and trimetallic cores were eventually produced from single-metal cores after years of material development. It has been discovered that the framework of the MOF can be damaged by including different or identical metals in binary and ternary forms without damaging the MOF's framework or crystal structure since these metals comprise the core of the MOF structure .The synergistic insertion of multiple metals in MOFs has greatly enhanced electrocatalysis through the reduction of energy barriers ,inclusion of multiple redox active sites, and promotion of increased conductivity for batteries and supercapacitors [12].

Furthermore, when used directly as electrode materials based on adding pseudo-capacitive redox centers, the bare MOFs can offer more active sites and a porous structure, encouraging fast ion transfer. Batteries, electrochemical supercapacitors, and electrocatalyst applications have all made substantial use of nanostructured materials composed of metal oxides and metal sulfides and high connectivity MOFs can be designed and synthesized [13]. Furthermore, a few papers in the literature have demonstrated that ligand elongation can significantly enhance MOF surface area and pore diameters. Chaitali R. Rawool et al. have synthesized Ni-BPDC by ultra-sonication method showing the specific capacitance of 69 F g^{-1} at 1 A g^{-1}, Nirmal Manyani et al. by hydrothermal method have synthesized Ni-BTC showing the specific capacitance of 193.05 F g^{-1} at 1 A g^{-1}, Chen Zhang et al. have synthesized Ni-MOF/MWCNTs with specific capacitance of 72.12 F g^{-1} by hydrothermal method. Guoyong Xiao et al. have synthesized Zn-Ni (MeIm)$_2$ by hydrothermal method showing the specific capacitance of 378 F g^{-1} at 1 A g^{-1} respective [14-20]. Using this method, MOFs' supercapacitive characteristics can be altered by creating MOFs with a different organic carboxylate link but the same metal core.

Due to their unique chemical and physical properties as well as their high Cs (specific capacity/capacitance), which is frequently several times much better than that of materials based on graphite/carbon, metal sulfides as possible electrode materials are currently being investigated. However, the poor rate performance and cycling stability of these sulfide electrodes prevent their use in practical applications. Building next-generation LIBs and SCs is made possible by nanostructures that have favorable transport properties, upon insertion/extraction high freedom for volume change, and other processes. These nanostructures also have high surface-to-volume ratios [21].

Here, we developed a simple, affordable, and scalable solvothermal technique to prepare five distinct sulphide-based Ni-MOFs, using five distinct linkers. The current study compares each of these MOFs based on their particle size, surface area, electrochemical conductivity, and structure analyzed by SEM, TEM, BET and XPS. The products can be utilized directly as electrode materials once they are prepared. The Ni-PM MOF electrode material exhibits the highest specific capacitance, energy density and largest surface area among all the prepared Ni-MOFs electrode materials. This work not only offers a crucial

concept for producing high-performing Ni-MOFs but also provides a further understanding about their structures and brief comparison of their properties because of different ligands and metal sulfate used.

1.2 Problem Statement

The main problem with electrode materials for pseudo capacitors is their low specific capacitance and Cyclic Stability, which limits the amount of energy that can be stored overall and results in materials with poor performance and limited practical use. Additionally, electrode materials often have poor cyclic stability, which degrades over time with repeated charge discharge cycles, reducing the longevity and performance of the device [22]. Furthermore, poor kinetics for charge transfer reactions are exhibited by certain electrode materials, which leads to slow charge-discharge rates and decreased device efficiency overall. Additionally, certain promising materials are expensive and hard to available, which makes it difficult for commercial pseudo capacitors to use them widely. The development of electrode materials for pseudo capacitors is further complicated by structural instability caused by volume expansion during cycling and environmental concerns [23]. The longevity and reliability of supercapacitors are eventually impacted by issues with the low conductivity, limited specific capacitance, and mechanical instability of Ni-MOF based electrode materials [24]. Ni-MOF's low conductivity and low electrochemical activity result in low specific capacitance and low power density when used as an electrode material for supercapacitors.

1.3 Research Hypothesis

The incorporation of rare earth metals like Zirconium and lanthanum and transition metal like Yttrium dopants into anatase TiO_2, and its combination with composite materials activated carbon and carbon nanotubes, hypothesized that these dopants would support conductivity, improve specific capacitance, and alleviate structural degradation. By introducing these Ni-MOFs, they predict a significant improvement in energy storage capabilities and cycling lifetimes, surpassing those achievable with conventional Ni-MOF based electrodes. Anticipate that this integration will further enhance conductivity, improve charge transfer kinetics, and support structural stability. Through systematic

4

experimentation and thorough electrochemical characterization, the target is to validate the hypothesis and contribute insights into the design and fabrication of advanced supercapacitor electrodes with superior performance and longevity

1.4 Research Objectives

The research conducted in this thesis mainly focuses on investigating and potentially developed high-performance supercapacitor electrode materials. The key objectives are as follows:

> ➢ To Synthesize Ni-MOFs that are both cost-effective and structurally stable.
> ➢ To obtain Electrode material with high energy and power density.

1.5 Scope of Study

Five different Ni-MOFs will be synthesized using various linkers as part of the project, and their structural, morphological, and compositional characteristics will be characterized using a range of analytical techniques. The study will assess the Ni-MOFs nanoparticles' electrochemical performance as stand-alone supercapacitor electrode materials. This entails evaluating rate capability, cyclic stability, and specific capacitance. Optimizing these electrodes' composition and manufacturing parameters will be the main goal of the project. This will entail evaluating energy storage capability and conductivity. The created Ni-MOFs electrodes' respective performances will be compared. This will assist in assessing the viability and efficiency of the suggested strategy for improving cycling lives and energy storage capacities. Along with offering insights into the design and manufacturing of sophisticated supercapacitor electrodes, the study will address the difficulties of the findings and offer suggestions for possible future research directions, including electrode topologies for even greater advancements

CHAPTER 2: LITERATURE REVIEW

2.1 Energy Storage Devices Overview

The need for efficient energy storage systems is growing as more and more green and renewable energy sources are being used. Numerous studies have been conducted recently to develop energy storage devices with high power densities, debilitated energy densities, long-term cycle stability, and safe operation. These include batteries, fuel cells [24,25], capacitors, and supercapacitors, the latter of which is of particular interest. One of the more recent versions of electrochemical energy storage devices is the supercapacitor. Their principles of operation and charge storage are more similar to those of rechargeable batteries. They are a favored choice for future electrical energy storage due to their outstanding performance. Supercapacitors and other energy storage devices, like batteries, are being used more often. Therefore, it is believed that they could provide an electrochemical energy storage technology alternative to commercially existing rechargeable batteries, especially lithium-ion batteries [26].
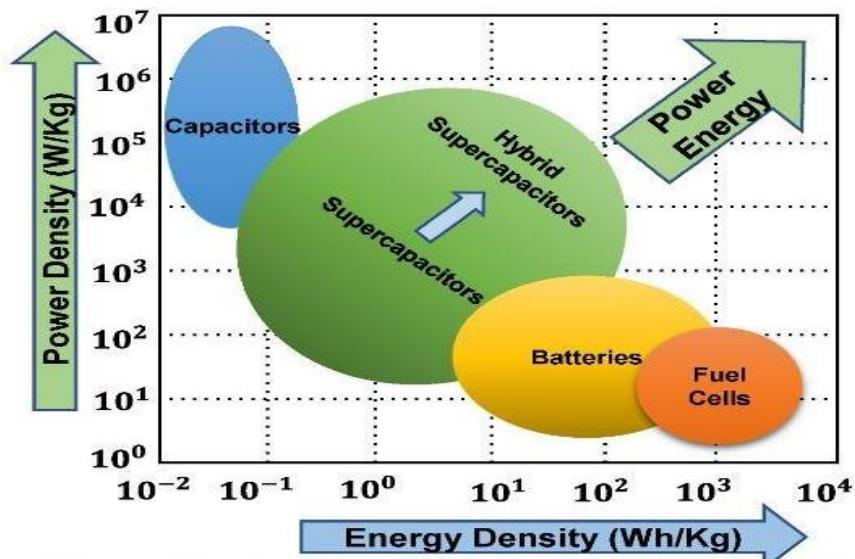
Figure 2. 1 Comparison of Energy and Power Densities of Energy Storage Device [28]

2.1.1 Batteries

Batteries balance energy density and power density by storing energy through chemical reactions.[29]. Many various applications, including electric cars and portable electronics, commonly use them [30]. Among batteries, lithium-ion batteries are the most well-known. Although adding solid state alternatives has enormous potential to increase energy and power densities, more development is necessary to get over issues with lifetime, rapid charging, and cost constraints [31]. During a Li-ion battery's discharge, Li+ moves via an electrolyte toward the cathode, and during charging, it moves from the cathode to the anode. Graphite anode and intercalated lithium compound (e.g., spinel $LiMnO_2$, layered oxide $LiCoO_2$, polyanion $LiFePO_4$, etc.) cathode comprise a typical lithium-ion battery. Lithium salts $LiClO_4$, $LiPF_6$, $LiBF_4$, and others are present in the electrolyte, which is a non-aqueous organic solvent. Lithium-ion cells [32-34].
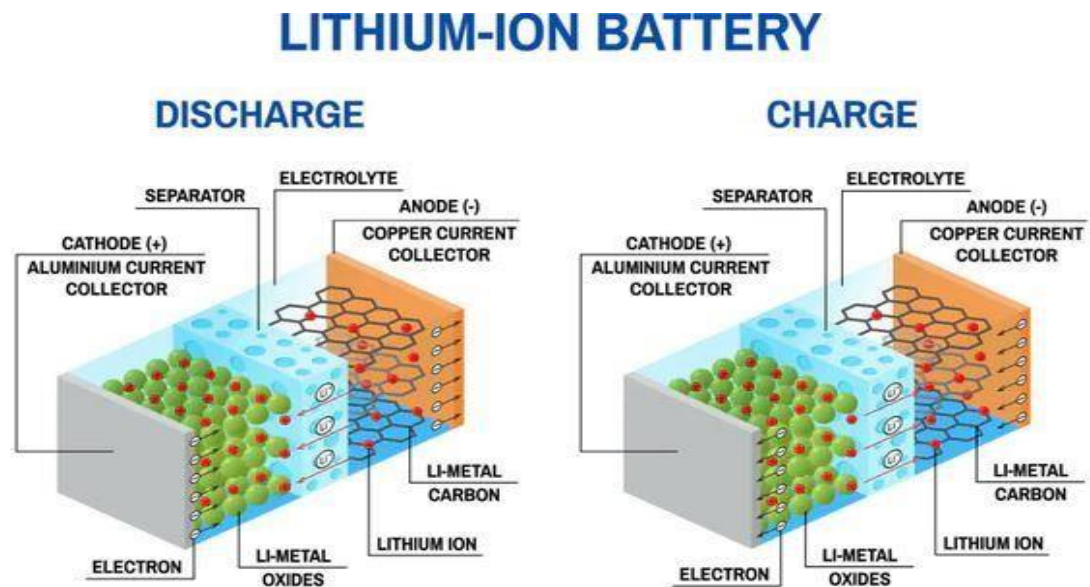
Figure 2. 2 Working principle of Lithium-ion batteries [35]

2.2 Supercapacitors Overview

Supercapacitors, also known as ultracapacitors, are charge storage devices that are superior to ordinary capacitors since they have a much lower voltage limit and a charge storage capacity of more than 5 KF. When compared to other devices, supercapacitors provide many advantages, including low cost, safe operation, notable power density values, exceptional cycle performance, and quick charging and discharging rates. They have been used in many different fields, such as power supply systems and electrical gadgets. The one drawback is that supercapacitors have relatively low energy density values. One of the two methods listed below could be used to resolve these problems:

    i.   The development of high-specific capacitance electrode materials

    ii.   Expanding the voltage window through additional electrolyte selection [36-37].

2.3 Types of Supercapacitors

They are differentiated according to the mechanism of storing energy:

    i.   Electrostatic double-layer capacitors

    ii.   Pseudo-capacitors

    iii.   Hybrid-capacitors

2.3.1 Electrochemical Double Layer Capacitors (EDLCs)

At the intersection of the electrode and electrolyte, a bilayer of electric charges is formed. Energy storage is caused by this phenomenon. Supercapacitor electrodes of the EDLC type include graphene, carbon aerogel, carbon nanotubes, AC, and others. As seen in Figure 1.4, the charging accumulator of a two-plate EDLC capacitor is situated at the interface between the electrode and the electrolyte. One can see this simply examining the diagram. The external circuit is used to move electrons from the negative electrode to the positive electrode during the charging process. The precise mechanism that attracts the electrolyte's cations and anions to match oppositely charged electrodes is unknown. During discharge, the motions of the electrons and ions counteract each other.
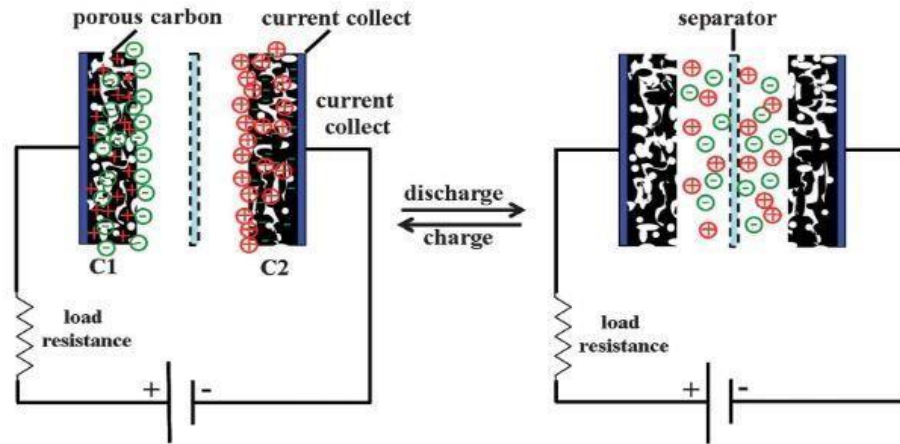
Figure 2. 3 Schematic illustration of how pseudo capacitor's function [38]

When compared to other capacitors, the formation of a Helmholtz electric bilayer causes the charge to be stored and separated extremely little [39]. On the outside of electrodes, charges build up when a voltage is applied to excite the cell. Ions of the electrolyte collect at the interface of oppositely charged electrodes because of the attraction between opposite charges caused by this potential difference. This causes a bilayer to form at the electrode-conducting solution junction. The electrolyte's oppositely charged ions diffuse onto the electrode surface after passing through the separator to balance this mixture [40].

2.3.2 Pseudo-Capacitors

Pseudo capacitors store energy through electron transport between the active electrode material and oxidation reduction processes. Transitional metal oxides (TMOs) such as RuO2, Mn2O3, and nickel oxide, as well as conducting polymers like PEDOT and polypyrrole PPy, are the components of a pseudo capacitor. These species' redox transitions and oxidation reduction processes are what give pseudo capacitors their capacity to store charge. Most of the supercapacitor rescinding is made up of pseudo capacitors. The behavior of pseudo capacitors is like that of batteries. These capacitors experience faradic reactions, much like regular batteries, and the electrochemical charge transfer is what causes the capacitance. Like batteries, pseudo capacitors also undergo intercalation and deintercalation of charges; however, the electrolyte's utilization increases power density

9

efficiency [41]. They are the perfect option for energy storage devices because they are less expensive and have a higher energy density than EDLCs. However, they also have low power densities and low cycle stability because of the reversible faradaic processes, exactly like batteries. Carbon materials, which have exceptional power densities and amazing cycle stability, are paired with pseudo capacitor-based electrode materials to address this problem [42].
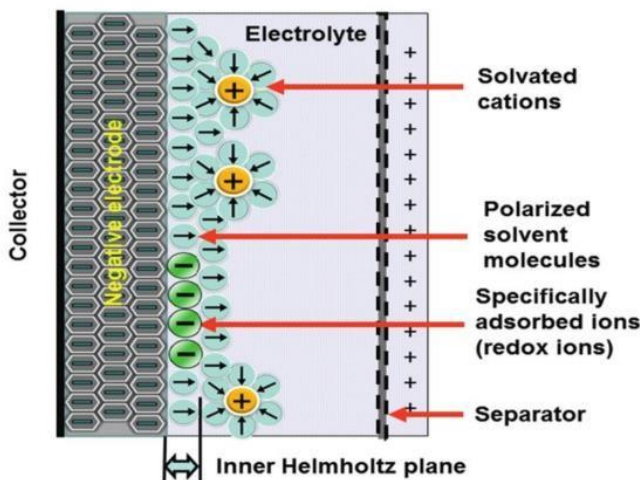
Figure 2. 4 Schematic diagram of working of pseudo capacitors.[43]

2.3.3 Hybrid Capacitors

These capacitors benefit from the characteristics of EDLCs and pseudo capacitors. Charge is stored in these capacitors because of redox processes and the development of an electric double layer. It is feasible to create a supercapacitor with capacitor-like characteristics (such as notable energy and power density values) and cyclic stability by combining the right electrode materials. Based on electrode designs, three different kinds of hybrid capacitors have recently been the subject of research. These include [44].

    i.   Battery type hybrids

   ii.   Composites hybrids

  iii.   Asymmetric hybrids

2.4 Electrode Material

The properties and electrochemical behaviors of supercapacitors are dependent on the electrode material. Therefore, materials for electrodes for supercapacitors have been divided into three main types [45,46].

    i.   Conducting Polymers

    ii.   Carbon materials

    iii.   Metal oxides

    iv.   Metal hydroxides

    v.   Nanostructures

2.4.1 Carbon Material

Electrochemical double layer capacitors are made with this. Charge is stored in EDLCs due to the formation of a bilayer at the interface between the electrode and conducting fluid. Because the method creates an electric bilayer, a material's surface property, a material utilized to create EDLC-type supercapacitors needs to have a large surface area. Materials made of carbon have a great conductivity, good mechanical stability, and a big surface area. They are therefore a perfect option for EDLC electrode materials. Carbon aerogel is the most common carbon material used in supercapacitors [45], graphene [46], activated carbon [47] carbon nanotubes [48], carbon nanosheets [49], etc. Although carbon-based electrode materials offer superior power density and stability, there is a little disadvantage. The primary issue with supercapacitors is their low energy densities, which arise from the surface process used for charge storage in these materials. This might be fixed, though, by combining carbon-based materials with other kinds of materials, such as conducting polymers or metal oxides, which would offer an effective power density. These kinds of electrode materials are referred to as composites or hybrids [50].
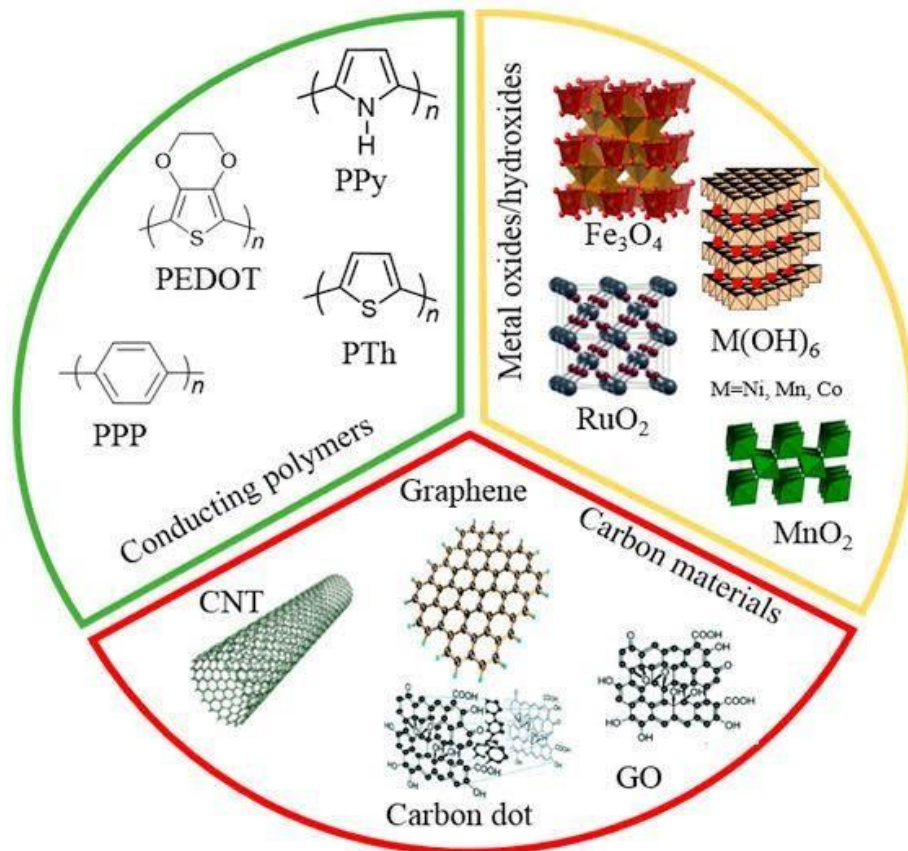
Figure 2. 5 Classification of electrode materials for supercapacitors [51]

2.4.2 Conducting Polymers

These are yet another class of materials that show promise for usage as electrodes in pseudo capacitors. Because of their quick and reversible redox changes, they exhibit pseudocapacitive behavior. Compared to carbon-based electrode materials, which have charge processes that affect the entire polymer mass in addition to the surface, they have superior conductivity and high capacitance values. Additionally, these materials often have quick charge-discharge processes [52]. They are also reasonably priced, which makes them a great option for supercapacitor electrode materials. PANI (polyaniline) is one of the most widely utilized conducting polymers [53], PEDOT (polyethylene dioxythiophene) [54], PPy (Polypyrrole) [55], PPP (poly paraphenylene) [56], and PTh (polythiophene) [57], etc. Chemical polymerization or electrochemical oxidation are the two methods used to create them. However, the phenomenon of swelling (during insertion) and shrinkage (during

disinsertion) of fibers during the charge discharge process causes mechanical stress in the polymer structure, which results in low cycle stability. Combining them with carbon-based materials, such as carbon nanotubes (CNTs) or graphene nanoplatelets (GNP), resolves this problem [58].

2.4.3 Transition metal Oxides

Rapid oxidation-reduction reactions cause this kind to exhibit pseudocapacitive behavior. Supercapacitors with high power densities can be made using metal oxide-based electrode materials since they have low resistance and high specific capacitance. Several oxidation states are present in transition metals. By altering their oxidation states during oxidation reduction reactions, they have a larger capacity to store charge. The crystal lattices of metal oxides are another factor contributing to their high specific capacitance. Since their crystalline forms increase conductivity, electrode materials based on metal oxides exhibit effective super capacitive performance. Various TMOs have been tested by researchers for making pseudo capacitors e.g., RuO_2 [72], NiO [73], Mn_3O_4 [74], TiO_2 [59-62], Fe_3O_4 [63], Co_3O_4 [64],[65], MoO_3 [66], MnO_2 [67], IrO_2 [68], Co_2O_3 [69] and MoO_4 [70] etc. RuO_2 has shown itself to be the most effective of these materials for supercapacitor electrodes. It provides outstanding cycle stability along with a high specific capacitance. However, employing RuO_2 is not cost-effective because it is a rare and expensive transition metal [71], [72]. As a result, attempts are underway to move toward affordable transition metal oxides that perform on par with RuO_2. Because of their exceptional qualities, binary metal oxides, particularly those of nickel and manganese have attracted the most attention in this context [73].

2.5 Electrolytes used for Supercapacitors

The type of electrode material used has a major impact on the performance of super capacitors. It is crucial to choose the appropriate electrolyte and an electrode material with a large surface area [74],[75]. Metal oxides, conducting polymers, graphene, carbon nanotubes, and activated carbon make up much of the supercapacitor electrode. Carbon nanostructures have been the primary focus of recent studies on electrolyte materials.

However, materials are based on graphene. Supercapacitors employ either liquid or solid electrolytes [76].

2.6 Different techniques for analyzing the behavior of Supercapacitors

The following are some of the techniques used to study the electrochemical behavior of supercapacitors.

2.6.1 Cyclic Voltammetry (CV)

Cyclic voltammetry is a technique that can be used to understand the specific capacitance of various materials. In addition to these, other electrochemical characteristics can be assessed, such as the electrode's electrochemically active surface area, diffusion coefficient, etc. Three electrodes—a working electrode, a Pt wire, and a silver electrode—are used to record cyclic voltammetry profiles. Additionally, suitable electrolyte is utilized. Various sweep rates are used to record CV profiles. The curve's shape indicates the type of supercapacitor; for instance, EDLCs produce a flawless rectangular CV curve, but pseudo capacitors show noticeable oxidation and reduction peaks. The capacitance can be calculated using the area under the curve. When the scan rate drops, the capacitance (specific) value of various materials rises [77,78].

2.6.2 Galvanostatic Charge-Discharge (GCD)

This method is used to assess the prepared electrodes' cyclic stability and to investigate the charge and discharge behavior of the electrodes. A working electrode, a Pt wire, and a silver electrode make up the electrode system in which it is also carried out. Additionally, a suitable electrolyte was utilized. Like cyclic voltammetry, the form of GCD curves indicates the kind of supercapacitors and how they behave. For example, the GCD curves for electrochemical double layer capacitors are symmetric and shaped like a perfect triangle. The oxidative-reductive behavior of the materials used for the pseudo capacitor electrodes, however, causes the curves in the case of pseudo capacitors to be asymmetric. GCD curves are captured at various current density values. To evaluate capacitance, the discharge time is necessary. It is also possible to examine the cyclic stability of electrode materials using the chronopotentiometry approach. To do this, the chronopotentiometry

14

approach is run for a few cycles at a given current density, and the capacitance retention for those cycles is then calculated [79,80].

2.6.3 Electrochemical Impedance Spectroscopy (EIS)

It is employed in the research of intrinsic qualities. In this instance, Nyquist plots with a frequency range from higher to lower are drawn between Zimg and Zreal in either acidic or alkaline conditions. The values of Warburg impedance, charge transfer resistance, ohmic resistance, and other parameters are then determined using the figure. A superior supercapacitor electrode material should have low charge transfer resistance and ohmic resistance values [81-84].

CHAPTER 3:   REVIEW ON EXPERIMENTATION METHODS AND CHARACTERIZATION TECHNIQUES

3.1 Synthesis Method

In disciplines like organic chemistry, materials science, and medicines, the ability to synthesize molecules from simpler components is crucial. Important methods include cyclization (e.g., Diels-Alder reaction), cross-coupling (e.g., Suzuki coupling), addition reactions (e.g., hydrogenation), elimination reactions (e.g., dehydrohalogenation), substitution reactions (e.g., SN1 and SN2), and functional group interconversion (e.g., alcohols to ketones). Solid-state synthesis, the sol-gel process, hydrothermal synthesis, chemical vapor deposition (CVD), and precipitation processes are examples of inorganic synthesis techniques. The material is synthesized in the current work using a hydrothermal technique.

3.1.1 Hydrothermal synthesis route

In a sealed container called an autoclave or hydrothermal reactor, hydrothermal synthesis is a flexible technique used to create a wide range of materials, such as nanoparticles, ceramics, and crystalline compounds. Reactants, usually metal salts, metal oxides, or organic compounds, are dissolved in water or another appropriate solvent to start the process. After that, the solution is put into the autoclave, where it is heated to high pressures and temperatures—usually between 100°C and 300°C—to create a regulated environment that promotes quick nucleation and growth. Particle size, shape, and crystallinity can all be precisely controlled as the reaction progresses over time, usually from hours to days. After finishing, the autoclave is cooled gradually, and the synthesized material is extracted from the solution—usually after contaminants have been washed off. Because of its ease of use, affordability, and environmental friendliness, hydrothermal synthesis is a popular technique in disciplines like environmental science, materials science, and nanotechnology for customizing the characteristics of functional materials for

uses [85]. For the analysis and characterization of materials the following techniques were used:

1. XRD (X-ray diffraction)

2. SEM (Scanning electron microscopy)

3. EDX (Elemental dispersive x-ray spectroscopy)

4. XPS (X-ray photoelectron spectroscopy)

5. FTIR (Fourier Transform Infrared Spectroscopy)

6. RAMAN spectroscopy

7. Brunauer-Emmett-Teller (BET) and pore size using Barret-Joyner-Halinda (BJH)

The materials' electrochemical characteristics and suitability for charge-discharge applications in supercapacitors were investigated. These are the primary electrochemical methods.

1. CV (Cyclic Voltammetry)

2. GCD (Galvanostatic charge-discharge)

3. EIS (Electrochemical impedance Spectroscopy)

3.2 Characterization technique

3.2.1 X-Ray Diffraction (XRD)

Since it provides information about the material's shape, composition, and crystallite size, X-ray diffraction, or XRD, is a crucial tool for material characterization. To complete the process, the X-ray radiation must be sent through the material at an angle. The measurement of the diffraction angle and intensity, which yields details about the structural morphology of the material under investigation, is the next step. Regarding crystalline materials, X-rays can exhibit two distinct behaviors in X-ray diffraction (XRD) patterns: as particles and as waves.

Identifying and characterizing materials based on their X-ray diffraction patterns is the primary goal of the technique being used. They make use of this technology. Diffraction is the term for the phenomena that occurs when a monochromatic X-ray beam strikes a substance. The Law of Bragg governs this phenomenon. Both constructive and destructive interference are features of crystalline structures. The atoms that make up the material are the source of this disturbance.

$$n\ (\lambda) = 2d\ \text{Sin}\ (\theta) \qquad\qquad (3.1)$$
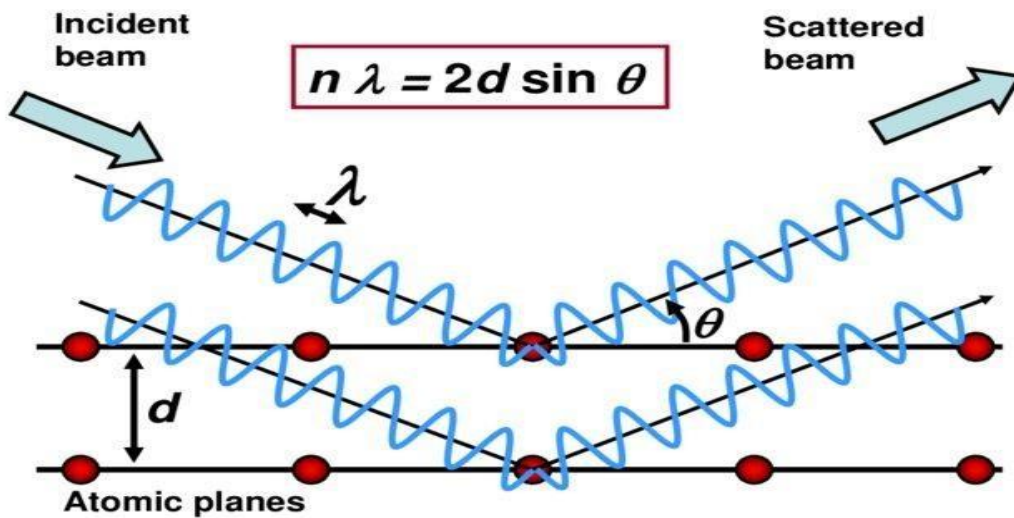
Figure 3. 1 Bragg's Law [86]

The arrangement of the atoms inside the crystal lattice affects the intensity of the diffracted waves, and the size and shape of the unit cell in the material dictates the potential directions of diffraction. Numerous small crystallites organized in different orientations make up a wide spectrum of materials. These crystallites are known as aggregate or polycrystalline powder. Anytime an X-ray beam strikes a material, it interacts with every

available interatomic plane. By changing the experimental angle, this interaction enables the identification of every diffraction peak.

3.2.2 Scanning Electron Microscopy (SEM)

A high-energy electron beam is used in scanning electron microscopy (SEM) to produce a range of signals on an object's solid surface. These electrons can travel through the substance and come out on the other side, as seen in **Figure 3.2.** The material's crystalline structure, surface appearance, material orientation, and chemical makeup can all be inferred from the interactions that occur between the electron beam and the sample. Usually, the SEM produces two-dimensional images that show spatial variations in the material's surface characteristics.

The basic scanning electron microscope (SEM) technology can differentiate between areas that are between 1 cm and 5 microns in size with magnifications ranging from 20X to 30,000X and a three-dimensional resolution of 50 to 100 nm. This method is particularly useful for studying crystalline structures, determining crystal orientations (EBSD), and performing semi-quantitative or qualitative studies of chemical components (EDS). In terms of both architecture and function, this scanning electron microscope (SEM) is similar to EPMA and can perform specific region or point location examinations on samples [87]. It works by using electromagnetic lenses and apertures to steer a concentrated beam of high-energy electrons at the sample from an electron cannon. The sample surface is scanned in a raster pattern by the tightly focused electron beam. The beam produces a variety of signals, including as characteristic X-rays, backscattered electrons (BSE), and secondary electrons (SE), as it interacts with the atoms in the sample. While backscattered electrons, which are reflected off the sample, provide compositional contrast because of their sensitivity to changes in atomic number, secondary electrons, which are expelled from the outer shells of atoms, provide high-resolution pictures of surface topography. With Energy Dispersive X-ray Spectroscopy (EDS), elemental analysis is made possible by characteristic X-rays that are released when electrons in the sample atoms change energy levels.

These signals are picked up by detectors in the SEM and processed to create detailed images with pixel intensities that correspond to signal strength. While certain versions provide low vacuum or variable pressure operation for non-conductive or hydrated samples, SEM functions under high vacuum settings to shield the electron source from electron scattering by air molecules. SEM's versatility makes it useful in many different sectors, such as biology for investigating cellular morphology, material science for analyzing microstructures, semiconductor inspection, forensic investigations, and nanotechnology for describing nanomaterials and structures.
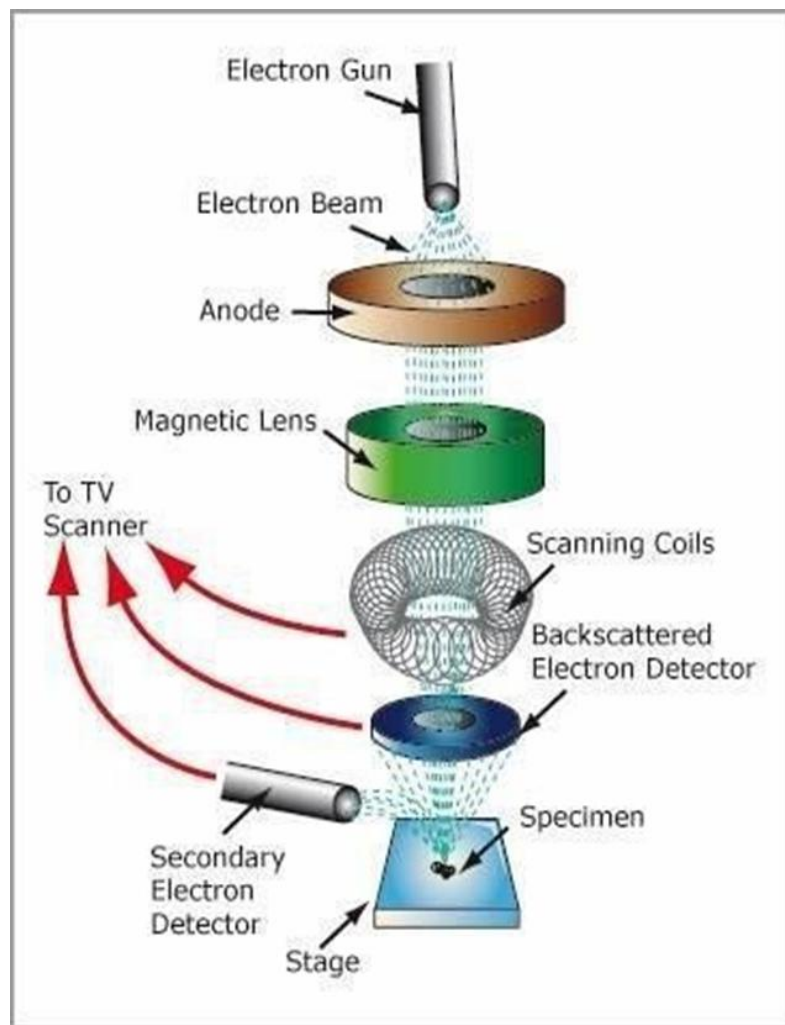
Figure 3. 2 Illustration of how SEM works [88]

3.2.3 Energy Dispersive X-ray Spectroscopy (EDX)

EDX is an effective method for elemental analysis that enables the quantification of elements in nanoparticles. It gives counts of elements at certain points in time rather than total numbers. To investigate nanostructures, EDX is commonly employed in combination with SEM or TEM. When EDX was first released as a commercial product at the start of the 1970s, it swiftly overtook WDS in popularity. The sensor's simple structure, which lacks any moving parts like the rotation detector employed by WDS, allows it to concurrently record X-ray energy signals from every constituent in a sample. As a result, the sensor can do analysis faster.

As a result, the sensor can do analysis faster. In comparison to WDS, EDX has a somewhat lower energy dispersion resolution, ranging from 150 to 200 eV. The lightest visible element is not carbon (C, atomic number 6), but rather oxygen (O, atomic number 8). Nevertheless, the benefits of lower expenses and quicker analysis more than offset these disadvantages.[89]. The EDX spectrum, which spans 0.1 to 10-20 keV, shows both light and heavy elements due to the existence of visible M or L lines of heavy elements and K lines of light elements.
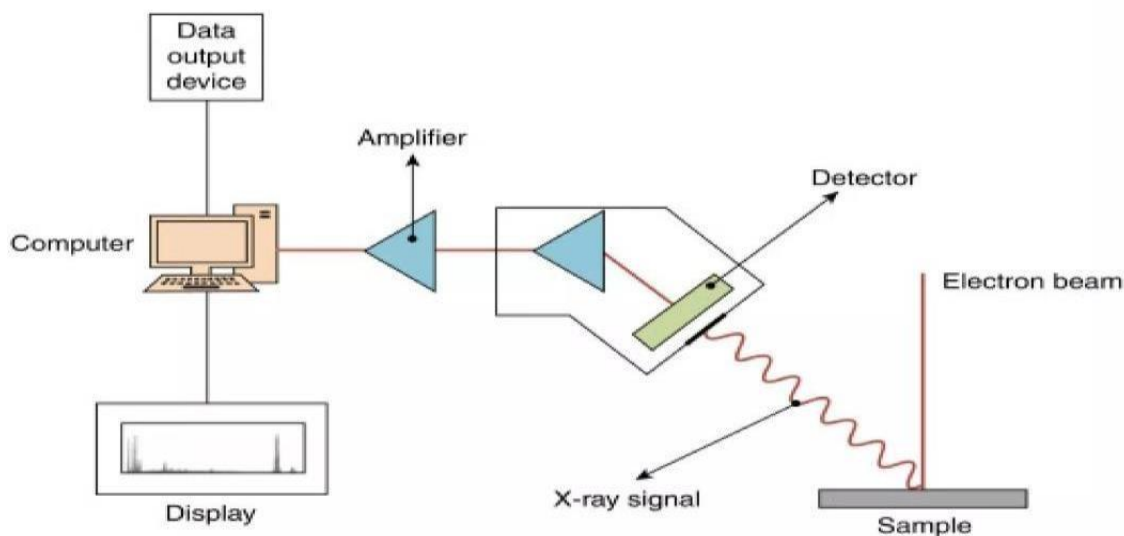
Figure 3. 3 Illustration of working principle of EDX [90]

3.2.4 Electron Spectroscopy using X-rays (XPS)

Surface analysis, or XPS for short, is a method used to determine the chemical makeup of different materials. A sample's surface is bombarded with X-rays, which causes the atoms there to release electrons known as photoelectrons. This is what allows the instrument to work. The properties of these photoelectrons are then ascertained by analyzing their kinetic energy and emission angles. Usually, the X-ray beam's energy is set to be higher than the electrons' binding energy in the sample's valence band. A positively charged ion can be created when X-ray photons expel one electron from the valence band through the process of absorption.

The electronic structure of the atom, including its chemical composition and bond state, can be determined by measuring the kinetic energy of these emitted photoelectrons using an electron analyzer. Elements inside a sample, along with their oxidation states and chemical environments, can be determined using XPS. Because of its high sensitivity, it can identify even the smallest contaminants or pollutants on surfaces. XPS is widely used in many different domains, such as materials science, surface chemistry, and semiconductor research, to characterize the surfaces of different materials [91]. The kinds

of samples that can be examined may be limited by the fact that XPS only analyzes the surface layers and necessitates high vacuum conditions, although offering extremely sensitive and quantitative surface analysis. Notwithstanding these drawbacks, XPS is nevertheless a potent instrument for in-depth surface characterization in material science, chemistry, and engineering.

In the top 1–10 nanometers of the surface, the resulting spectrum shows peaks that correspond to various binding energies, giving quantitative information about the elemental composition and chemical states of the elements.
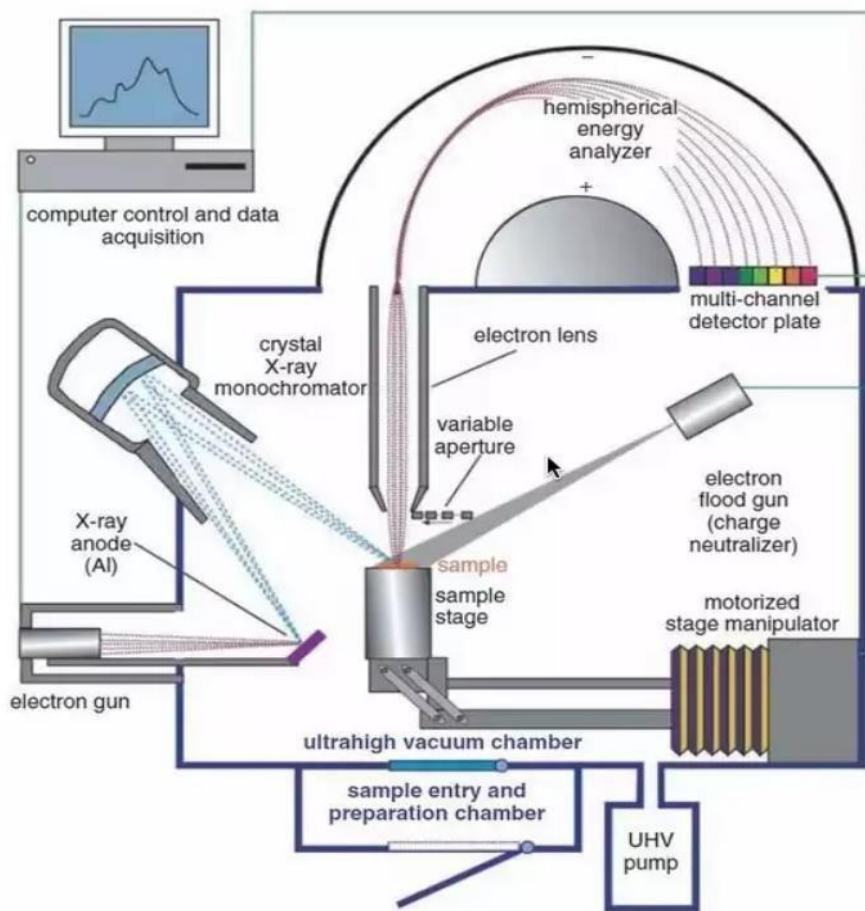
Figure 3. 4 Working Principle of Electron Spectroscopy using X-rays [92]

3.3 Electrochemical Techniques

After preparation of slurry and 30 minutes sonication at room temperature, the nickel-based electrode is put through electrochemical testing. The electrochemical workstation for supercapacitors uses three main techniques:

      i.   Cyclic Voltammetry (CV)

      ii.   Chronopotentiometry Measurements

      iii.   Electrochemical Impedance Spectroscopy (EIS)

3.3.1 Voltammetry in Cycles

Cyclic voltammetry is a widely used electrochemical technique for analyzing the redox reactions of molecules. It is crucial for researching chemical reactions that are started by electron transport, such catalysis. This approach involves exposing two electrodes in the workstation to a certain range of potentials during a cycle. Parameters such as scan rate, sample interval, and sensitivity are changed for each run; a cycle has two halves. CV clarifies the relationship between current and voltage. The three-electrode system used in a beaker cell for this test consists of glassy carbon electrodes, Ag/AgCl electrodes, and platinum wire [93].

3.3.2 Chronopotentiometry

Chronopotentiometry is an analytical method in which the electroactive material steadily decreases because of electrodes experiencing a constant current flow. Compared to coulometric titrimetric and constant-current coulometry, this method uses a larger current, which quickly reduces the necessary current efficiency for material reduction to less than 100% in a couple of seconds.

3.3.3 Impedance Spectroscopy Electrochemical (EIS)

EIS is used to quantify the system's resistivity, which encompasses electrolyte resistance, ohmic loss, and activation losses. Electrical resistance is a measurement of a circuit element's resistance to current flow.

$$R = E/I \qquad (3.2)$$

According to Ohm's Law, resistance (R) can be calculated by dividing the voltage (E) by the current (I). Any range of current and voltage can be subject to this law, which is frequency independent. In a perfect resistor, the AC current and voltage are in phase.

3.4 Parameters of Electrochemistry

A supercapacitor's effectiveness must be assessed by looking at its energy and power densities. The two primary techniques for formula-based determination of these densities are cyclic voltammetry (CV) and chronopotentiometry:

The C_s (specific capacitance) ($F\ g^{-1}$) can be determined using cyclic voltammetry:

$$\mathbf{C_s\ (F\ g^{-1}) = } \quad A/2mK(\Delta V) \qquad (3.3)$$

In this instance, m represents mass, on the scan rate used for the analysis, and V the voltage window of the procedure. The integral area of CV curves is represented by $\int IdV$.

$$\mathbf{E_s = (C_s\ \Delta V^2)\ /2\ x\ 3.6} \qquad (3.4)$$

Here, E_s represents energy density. The power density is calculated as,

$$\mathbf{P_d = 3600\ E_s/\Delta t} \qquad (3.5)$$

Here, P_d represents the power density that can be achieved by a supercapacitor.

CHAPTER 4:   METHODOLOGY

4.1 Materials

All chemical reagents utilized were of analytical quality and don't require additional purification before usage. Nickle Sulphate hexahydrate ($NiSO_4 . 6H_2O$, purity > 99%), Benzene-1,3,5-tricarboxylic acid ($C_9H_6O_6$, H_3BTC, purity > 99%), Benzene-1,4-dicarboxylate ($C_8H_6O_4$, H_2BDC, purity > 99%), 2-Methylimidazole ($C_4H_6N_2$, MEIM, purity > 99%), 1,10-phenanthroline monohydrate ($C_{12}H_{10}N_2O$, Phen, purity > 99%), Polyethylene glycol (H-(OCH_2CH_2)n OH, PEG, purity > 99%) were all chemicals used in this synthesis process, purchased from Sigma Aldrich. Ethanol (EtOH) and N, N Dimethylformamide (DMF) were used as solvent, also procured from Sigma Aldrich (purity > 99%).

4.2 Methodology

Briefly, the Ni-MOFs were all prepared through simple solvothermal methods. For the synthesis of Ni-PM$_{(DMF)}$, the first solution was made by dissolving $NiSO_4.6H_2O$ (0.394 g, 1.5mmol) in 60 mL of DMF and stirred for 30 minutes while the second solution contained 1,10-phenanthroline monohydrate (0.270 g, 1.5 mmol) in 60 mL DMF also stirred for 30 minutes. After being stirred the homogenous solutions were mixed by first solution poured into second solution into 120 mL Autoclave with a Teflon lining and heated at 180 °C for 12 h. After cooling to room temperature, the resultant grey precipitates were accumulated by centrifugation, washed with DMF and ethanol three times, and then dried at 80 °C for 12 h. Similarly, Ni-BDC$_{(DMF)}$, (0.249 g, 1.5 mmol) (black), Ni-MEIM$_{(DMF)}$ (0.123 g, 1.5 mmol) (grey), Ni-BTC$_{(DMF)}$ (0.294 g, 1.5 mmol) (light green) and Ni-PEG$_{(DMF)}$ (3.964 g, 1.5 mmol) (dark gray) were synthesized using the same procedure while taking $NiSO_4.6H_2O$ (0.394 g, 1.5mmol). The schematic synthesis procedure was shown in Figure 4.1.
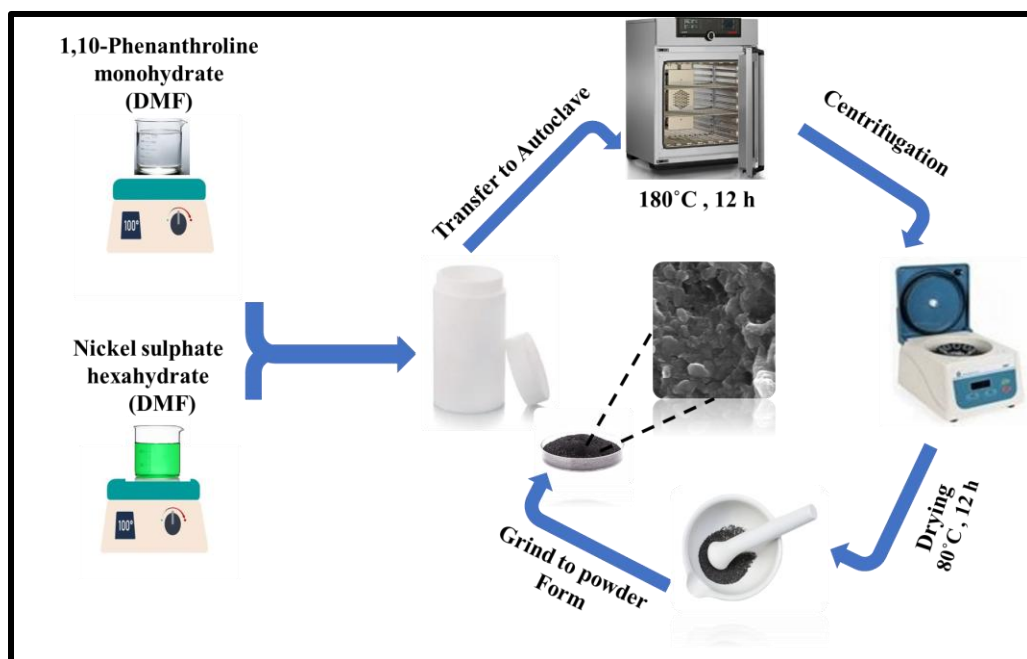
Figure 4. 1 Schematic diagram for the synthesis Ni-MOFs

4.3 Synthesis of post cycled electrodes for testing

The produced materials' structural changes were investigated using ex-situ XRD and SEM examinations. An X-ray diffractometer was used to analyze the material's phase crystallinity, and a scanning electron microscope was used to evaluate the cycled electrodes' morphology.

4.3.1 Preparation of working electrode

A homogenous slurry was prepared by combining 80 μl ethanol, 20 μl of binder (5% Nafion per solution of fluorinated resin solution), and 2 mg active ingredient while sonicated for half hour. Using a micropipette, drop of 1.5 μl on glassy carbon was cast and to prepare a functional electrode at room temperature was dried 5-10 minutes. For all electrodes in this case in electrochemical measurements, the mass loading was approximately about 2 mg.
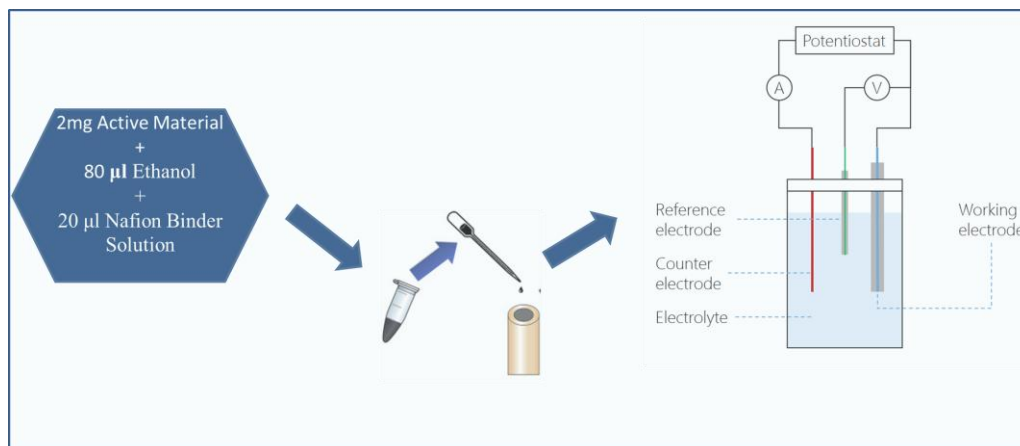
Figure 4. 2 Schematic diagram for the preparation of working electrodes

4.4 Electrochemical Studies

Electrochemical testing of the prepared electrodes was executed using CH Instruments' Electrochemical Workstation 660E. Three-electrode cell types were used for cyclic voltammetry (CV), galvanostatic charge–discharge (GCD), and electrochemical impedance spectroscopy (EIS). The reference electrode in the three-electrode setup was Ag/AgCl, while glassy carbon served as the working electrode's substrate and platinum wire as the counter electrode. Aqueous electrolyte of 3 M KOH was employed in the experiment. A homogenous slurry was prepared by combining 80 μl ethanol, 20 μl of binder (5% Nafion per solution of fluorinated resin solution), and 2 mg active ingredient while sonicated for half hour. Using a micropipette, drop of 1.5 μl on glassy carbon was cast and to prepare a functional electrode at room temperature was dried 5-10 minutes. Electrochemical testing of all the electrodes in electrolyte was done within the potential window of - 0.5V – 0.55V.

It was estimated that the mass loading for each electrode was 2 mg. CV profiles were seen at different scan speeds of 5, 10, 30, 70, and 100 mV/s, within a potential range of - 0.5 to 0.55 V. Chronopotentiometry was used to obtain GCD curves at different current densities of 0.5, 0.7, 1, 2, and 3A/g within the same potential window. Nyquist graphs were produced using EIS with an amplitude of 0.005 V over a frequency range of 1 Hz to 1 M.

CHAPTER 5:   RESULTS AND DISCUSSION

5.1 X-ray diffraction (XRD)

The prepared Ni-MOF's crystallinity and phase purity is confirmed by the XRD analysis findings. According to **Figure 5.1**, five different Ni-MOFs that were synthesized had discrete peaks ranging from 5° to 80°. The peaks of Nickle Phenanthroline monohydrate MOF (Ni-PM MOF) at 2θ of 7.21°, 10.62°, 11.87°, 15.5°, 21.79°, 27.3°, 31.54°, 44.45°, 51.94°, 56.36°, and 76.3° correspond to the typical diffraction patterns of Ni-MOF-74, ZIF-8 XRD and JCPDS 00-062-1030 [94-96]. Similarly, all other synthesized Ni- MOFs depict the same diffraction pattern as shown by Ni-PM MOF at same theta values with difference in intensity.

Table 5. 1 XRD parameters achieved for all prepared electrodes

Sample	2θ	d(nm)	FWHM°	Average Crystallite size (nm)
Ni-PM MOF	7.23, 31.51, 44.45	12.21, 2.83, 2.03	0.613, 0.376, 0.413	21.5
Ni-BDC MOF	7.25, 31.53, 44.45	12.18, 2.83, 2.03	0.418, 0.348, 0.409	23.2
Ni-MEIM MOF	7.27, 31.51, 44.47	12.14, 2.83, 2.03	0.354,0.331, 0.429	25.3
Ni-BTC MOF	7.19, 31.41, 44.45	12.28, 2.84, 2.03	0.492, 0.324, 0.323	26
Ni-PEG MOF	7.27, 31.41, 44.45	12.28, 2.84, 2.03	0.348, 0.324, 0.323	29

Some parameters of all the prepared electrodes in **Table 5.1** are enlisted. Average crystal size was found by Debye Scherrer formula given in Equation .10 showing the

average crystallite size of 21.5 nm, 23.2 nm ,25.3 nm, 26 nm and 29 nm by Ni-PM, Ni-BDC, Ni-MEIM, Ni-BTC and Ni-PEG MOF.

$$D = \frac{K\lambda}{\beta cos\theta} \tag{5.1}$$
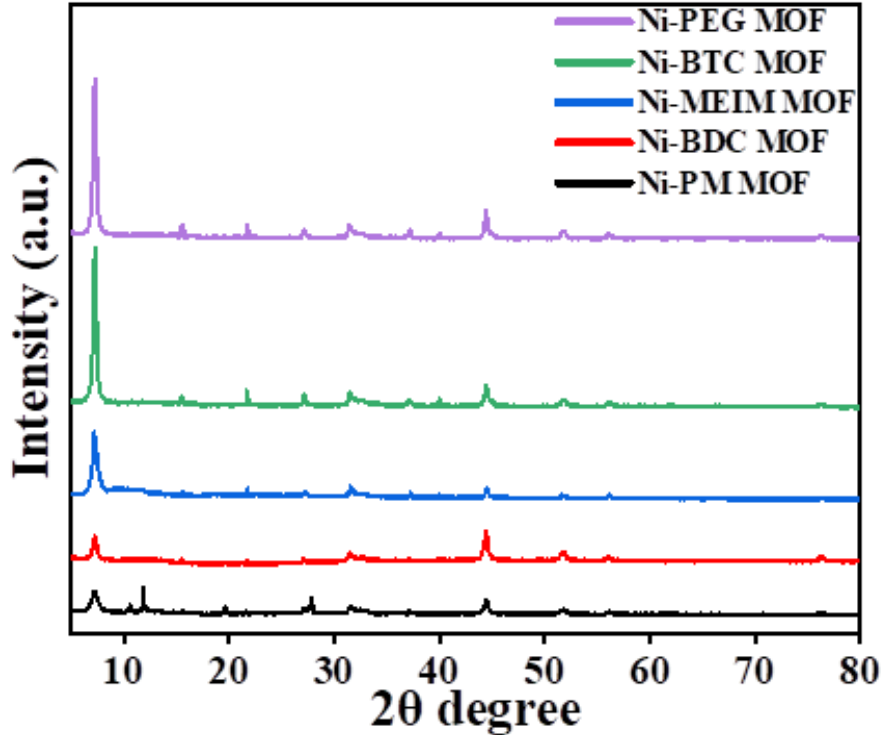
Figure 5. 1 XRD pattern of Ni-PM MOF, Ni-BDC MOF, Ni-MEIM MOF, Ni-BTC MOF and Ni-PEG MOF

5.2 Scanning Electron Microscopy

For the study of morphological characteristics of all the prepared electrodes, SEM analysis has been performed. In **Figure 5.2(a-e),** the surface morphology of all the prepared Ni-MOFS demonstrates diverse nanostructures with complex mesoporous networks of pores and channels in good agreement with the mesoporous size distribution given by N_2 adsorption-desorption isotherms. However, it was not possible to discern the discrete crystal units' size as the agglomerates of fused crystals were observed. In **Figure 5.2 (a)** Ni-PM MOF appears to have a rough, porous structure representing crumpled or flaky

morphology with high surface area. **Figure 5.2(b)** Ni-BDC MOF shows granular morphology composed of small individual particles**. Figure 5.2(c)** Ni-MEIM MOF shows nanoflower morphology with nanosheets stacked like flower petals. **Figure 5.2(d)** Ni-BTC MOF displays cloudy, interconnected structure representing fluffy or sponge-like morphology and **Figure 5.2(e)** Ni-PEG MOF appears as aggregated or clustered particles with rough morphology.
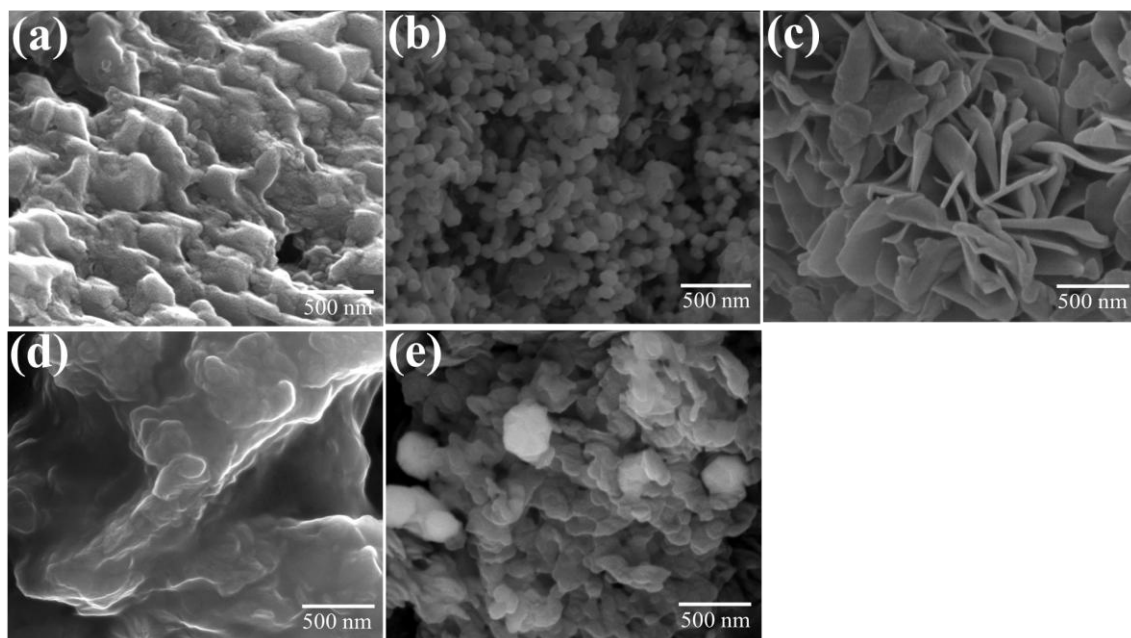
Figure 5. 2 SEM images; Ni-PM MOF (a), Ni-BDC MOF (b), Ni-MEIM MOF (c), Ni-BTC MOF (d), Ni-PEG MOF (e)

5.3 Elemental dispersive x-ray spectroscopy (EDX)

The presence of expected elements on the surface of all the prepared electrode's material has been confirmed by EDX analysis. EDX mapping in addition to EDX spectra of the prepared samples presented in **Figure 5.3 (a, c)** which shows the presence of Ni, O, N and C where the prepared samples' primary constituents' carbon and metal can be seen. The small amount of N that was visible may have come from the DMF solvent when DMF molecules were added to the Ni-MOFs that were prepared.
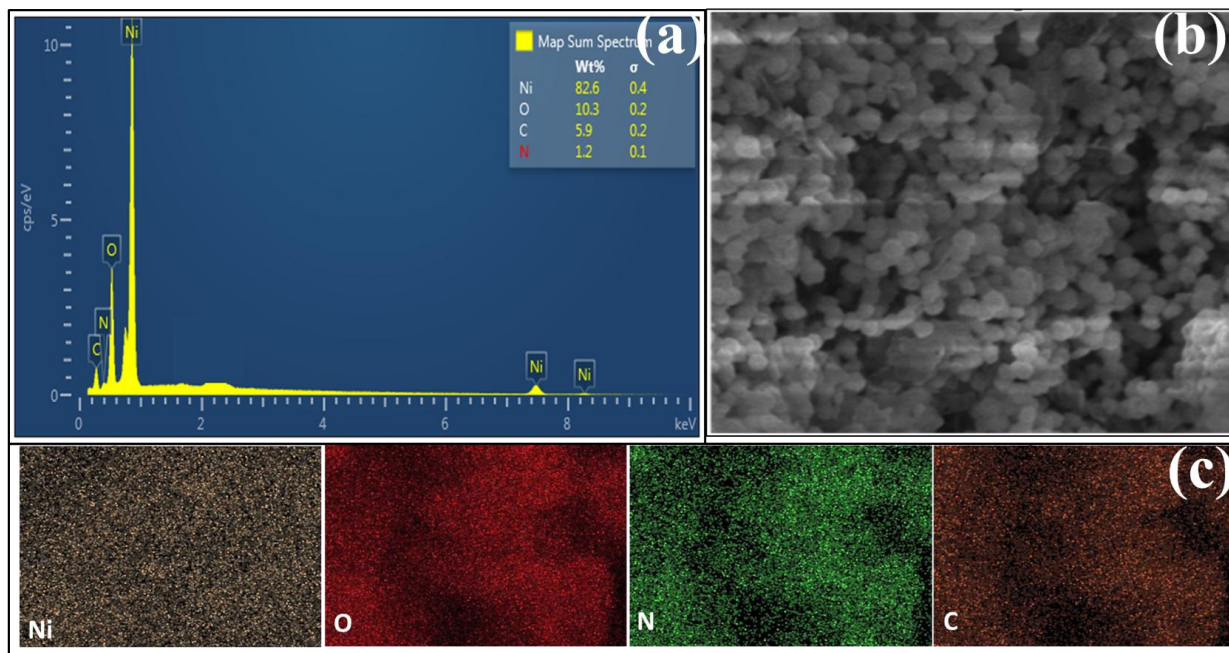
Figure 5. 3 (a, b, c) EDX mapping of Ni-PM MOF

5.4 Transmission Electron microscopy (TEM)

Figure 5.4(a) presents the image of TEM showing a high-resolution structural analysis of the best performing Ni-PM MOF. TEM analysis revealed agglomerated structure indicating that the material has rough, porous structure with multiple grains of various sizes and shapes, with some areas appearing lighter indicating the presence of carbon and darker (denser) a range of sizes of randomly scattered metal nanoparticles corresponding well with the SEM image of Ni-PM MOF in **Figure 5.2(a)**. **Figure 5.4(b, c)** represents an enlarged view along with the live profile. The identified lattice fringes with interplanar spacing d = 0.28 nm and 0.21 nm confirms the crystalline nature of the material, corresponds well to the interplanar spacing of Ni-PM MOF, and matched well with the corresponding diffraction data from XRD given in **Figure 5.1**.
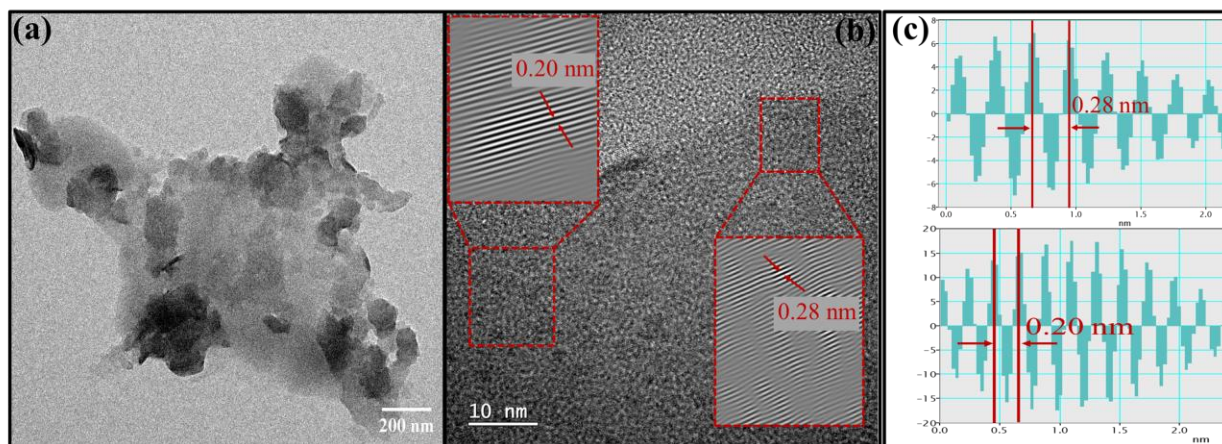
Figure 5. 4 (a, b) TEM image and (c) live profile of Ni-PM MOF

5.5 X-ray photoelectron spectroscopy (XPS)

The electron structure and elemental composition of the best sample as-prepared Ni-PM MOF is further characterized by XPS (X-ray photoelectron spectroscopy) measurements. The elements Ni, O, C and N were evidently detected by deconvoluted high resolution XPS spectra, as shown in **Figure 5.5**. Survey spectrum of Ni-PM MOF is presented in **Figure 5.5(a)**. Ni^{2+} and Ni^{3+} spectra shown in **Figure 5.5(b)**, showing two shake-up satellites and the fitting peaks at 855.6 eV and 872.9 eV correspond to Ni $2p_{3/2}$ and Ni 2p½ indicating the presence of Ni^{+2}, whereas the peaks at 856.3 eV and 874.3 eV corresponds to Ni $2p_{3/2}$ and Ni 2p½ indicating the presence of Ni^{+3}. Also, two additional strong shakeup-type peaks at 861.2 and 879.7 eV are Ni $2p_{3/2}$ and Ni 2p½ satellite peaks of nickel [97-100]. Similarly, as illustrated in **Figure 5.5(c)** the O1s spectra deconvoluted into three peaks each centered at 531.2 eV, 531.5 eV and 532.5eV [101-103]. These peaks are ascribed to the lattice hydroxyl groups, the C–O and C=O bonds separately. **Figure 5.5(d)** shows the deconvoluted C1s peaks with binding energies of 284.4 eV, 284.7 eV, and 285.5 eV corresponding to the C=C, C-C, and C-N bonds respectively [104-106]. **Figure 5.5 (e)** shows the N1s spectra of the sample. N1s spectra showed four deconvoluted peaks with binding energies of 398.8 eV,399.1 eV, 401.1 eV, and 401.6 eV representing C=N-C, C=N, N-H, and C-NH₂ [107-109].
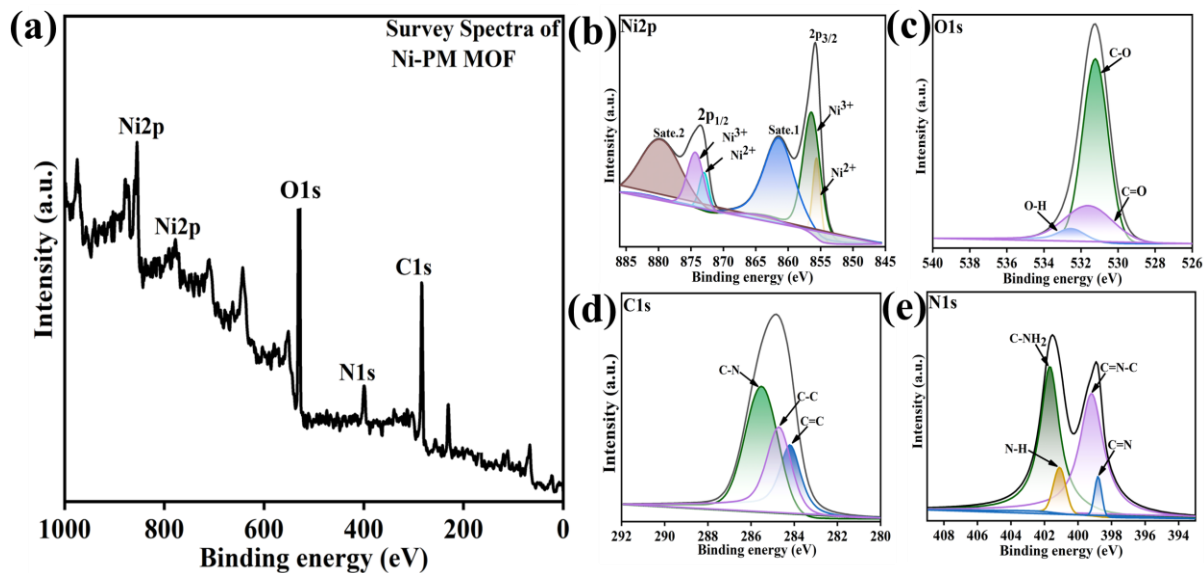
Figure 5. 5 (a) XPS survey spectra of Ni-PM MOF, (b-e) deconvoluted XPS spectrum of

Ni-PM MOF for Ni 2p, O1s, C1s and N1s.

5.6 Fourier Transform Infrared Spectroscopy (FTIR)

Figure 5.6(a) shows the FTIR spectra of five powdered Ni-MOFs. For Ni-MOFs, the peak indicating stretching vibrations of the O-H group are shown by Ni-PEG, Ni-BTC, and Ni-BDC MOF and N-H bond by Ni-MEIM and Ni-PM MOF at 3411 cm^{-1}. Furthermore, the C-H stretching bond present in the Ni-based materials is demonstrated by the peak for all synthesized Ni-MOFs at 2774 cm^{-1} respectively. The peak at 1634 cm^{-1} was attributed to O-H bending vibrations in Ni-PEG MOF, C=O in Ni-BTC and Ni-BDC MOF, and C=N in Ni-MEIM and Ni-PM MOF. The peak at 1468 cm^{-1} was assigned to C-H bending vibrations in Ni-PEG MOF and C=C stretching vibrations in Ni-BTC, Ni-BDC, Ni-MEIM, and Ni-PM MOF. The peaks in the range of 1233–1080 cm^{-1} are attributed to C-O stretching vibrations in Ni-PEG, Ni-BTC, Ni-BDC MOF, and C-N bond in Ni-MEIM and Ni-PM MOF. Similarly, the peaks at 862, 758, and 630 cm^{-1} represent the C-H bending vibration of linkers in synthesized Ni-MOFs. The peak at 483 cm^{-1} represents the stretching vibrational mode of Ni-O bond in Ni-PEG, Ni-BTC, Ni-BDC, and Ni-N bond in Ni-MEIM and Ni-PM MOF. These results provide strong support for the successful synthesis of Ni-

MOFs by the presence of expected functional groups or bonds aligned with the expected molecular structure [110-113].
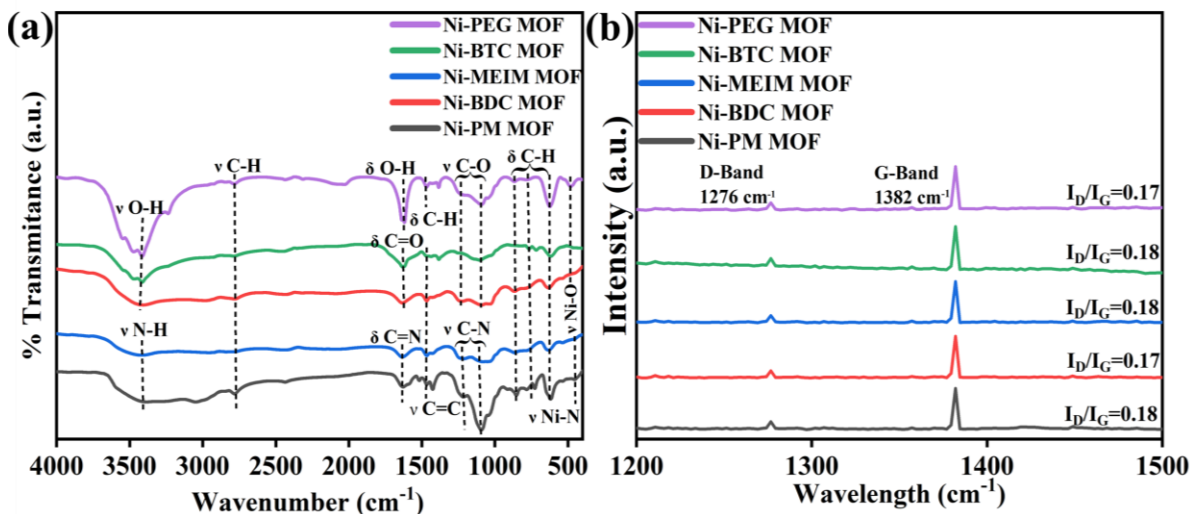
Figure 5. 6 (a) FTIR and (b) Raman spectroscopy of Ni-PM MOF, Ni-BDC MOF, Ni-MEIM MOF, Ni-BTC MOF and Ni-PEG MOF.

5.7 Raman Spectroscopy

The prepared samples Ni-PM MOF, Ni-BDC MOF, Ni-MEIM MOF, Ni-BTC MOF, and Ni-PEG MOF contained carbon confirmed by Raman spectroscopy. The ID/IG ratio, where ID is the D-band intensity and IG is the G-band intensity, is used to calculate the graphitization level. The synthetic five Ni-MOFs' Raman spectra are displayed in **Figure 5.6(b)**, where two strong D (disorder induced) and G (graphitic) bands can be seen. These bands are situated approximately between 1276 cm^{-1} and 1382 cm^{-1} showing the ligands C-C inter ring stretch at 1276 cm^{-1} and stretching in a coordinated C-O symmetry at 1382 cm^{-1} in line with the literature [114]. Additionally, the prepared electrodes ID/IG ratio based on the data is calculated to be 0.18 for Ni-PM, Ni-MEIM, Ni-BTC MOF, and 0.17 for Ni-BDC, Ni-PEG MOF. More graphitic or sp$_2$ carbon structure which is commonly associated with fewer structural defects and more crystallinity, is indicated by a low I_D/I_G ratio. One of the factors contributing to good specific capacitance is improved electrical conductivity, which is facilitated by a higher degree of graphitic carbon.

5.8 Brunauer-Emmet-Teller (BET) analysis

To analyze the surface area and pore radius of synthesized electrode materials, N_2 adsorption-desorption isotherms were studied as depicted in **Figure 5.8**. The mesoporous structures are confirmed by the type IV isotherms that each electrode displayed in **Figure 5.8(a)**, which included a characteristic hysteresis loop [115]. **Table.1** provides a summary of the BET outcomes. Among all the prepared electrodes, Ni-PM MOF has the largest surface area (24.387 m^2 g^{-1}), whereas Ni-PEG MOF has the lowest surface area (2.07 m^2 g^{-1}). When compared to all other prepared electrodes, as described and illustrated in **Table 5.2**, the derived Ni-PM MOF supercapacitor electrode's specific capacitance increased significantly due to an increase in surface area.
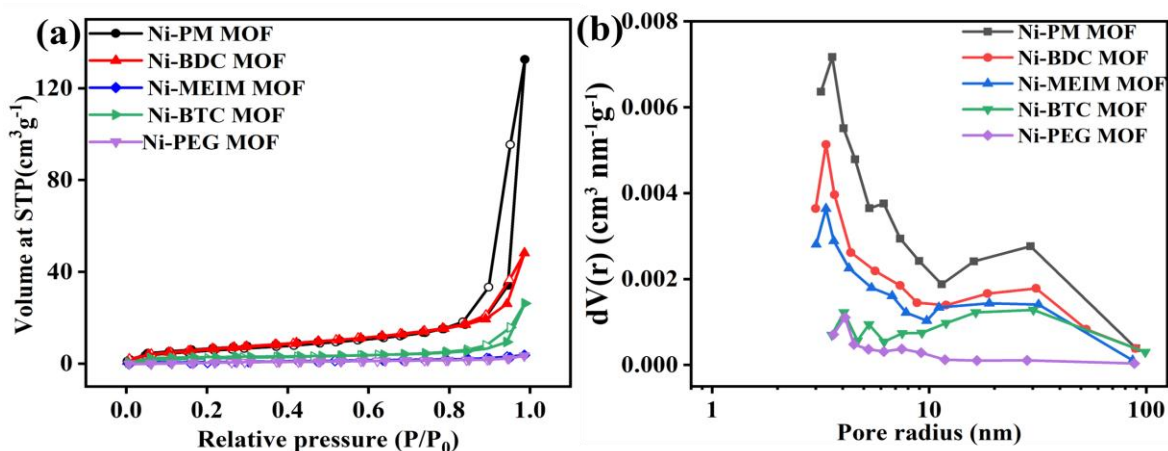
Figure 5. 7 (a, b) BET isotherm and Pore radius distribution of Ni-PM MOF, Ni-BDC MOF, Ni-MEIM MOF, Ni-BTC MOF and Ni-PEG MOF

From BJH adsorption method the pore radius is determined shown in **Figure 5.7 (b)**. It displays a typical mesoporous material's average pore radius between 3 and 50 nm. Improved electron and ion transfer at the electrode-electrolyte interface is dependent on the mesoporous structure of the prepared electrodes, which also provides an abundance of active sites for quick electrochemical reactions.

Table 5. 2 Surface area determined by BET, pore volume and size by BJH for the different samples.

Electrode Material	Surface area $m^2\,g^{-1}$	Pore radius (nm)
Ni-PM MOF	24.38	3.54
Ni-BDC MOF	24.08	3.34
Ni-MEIM MOF	19.47	3.35
Ni-BTC MOF	9.55	4.01
Ni-PEG MOF	2.07	4.07

5.9 Cycle Voltammetry (CV) Analysis

The prepared electrodes' redox process was examined using CV (cyclic voltammetry) analysis. CV analysis was performed at different scan rates between 5-100 mV s-1 CV curves of synthesized Ni-MOFs based electrodes are shown in **Figure 5.9(a-e).** CV curves depict pseudo-capacitive behavior. When the potential reaches a suitably negative/positive potential, an electrical current is produced. Initially, the potential is scanned linearly over time, causing a chemical specie (Nickle) to undergo oxidation or reduction at the electrode surface. An oxidative (or anodic) current is observed beginning at the onset potential of the redox event (where the background-subtracted current becomes non-zero) in an oxidation reaction, where oxidation of the redox-active specie takes place at the electrode surface as the electrode potential is scanned in a positive direction. Oxidation becomes more thermodynamically favorable as the potential rises through the greater than half potential of the redox-active metal, and the current keeps increasing until the oxidation process is finally constrained by specie diffusion to the electrode surface, producing a diffusional tail that is characterized by a decrease in the current. After then, the electrode's potential sweep is turned around and scanned in the opposite direction until the starting potential is attained [116]. The following peak current increases with scan rate, as demonstrated by CV curves, suggesting that the electrode material is performing well electrochemically.

From CV graphs performed at 5, 10, 30, 70, and 100 mV s^{-1} ECSA is calculated by using the following formula and shown in **Figure 5.9 (f)** [117].

$$ECSA = \frac{C_{dl}}{C_s} \qquad (5.2)$$

The double layer capacitance (Cdl) is calculated using the open circuit potential (OCP) of the non-faradic portion of CV curves

$$C_s = \frac{\int I\, dV}{2 \times V \times m \times \Delta V} \qquad (5.3)$$
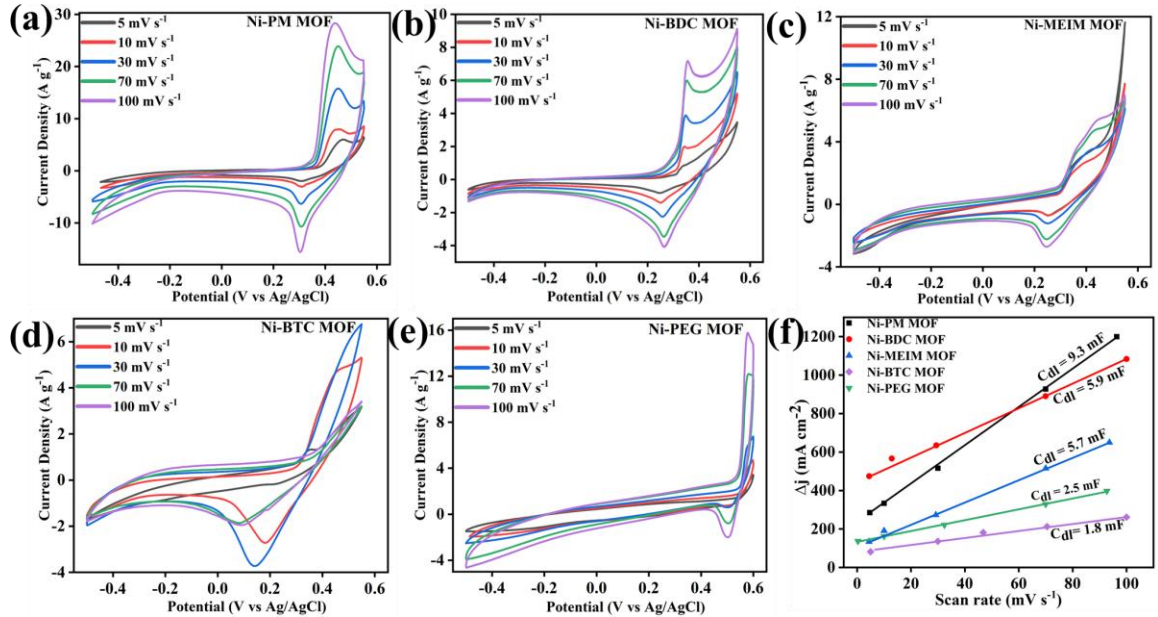
Figure 5. 8 (a-e) CV scans at scan rates 5, 10, 30, 70 and 100 mV s^{-1}, (f) Relation between capacitance and Scan rate of all prepared electrodes

To comprehend the electrode active materials better charge storage mechanism, Dunn's power-law approach was used. Generally, at a given voltage current can be divided into diffusion-limited current (i_{diff}) and capacitive current (i_{cap}).

$$i = i_{cap} + i_{diff} = k^1 v + k^2 v^{0.5} \qquad\qquad (5.4)$$

where k2 is the constant for diffusion-limited processes and k1 is the constant for capacitive processes. At a scan rate of 30 mV s^{-1}, **Figure 5.9.1 (a, b, c, d, e)** shows the percentage of current contributions from both diffusion-limited and capacitive processes. Less than 35% of the overall current contribution came from the diffusion process in Ni-PM, Ni-BDC and Ni-MEIM MOF, indicating the supremacy of the capacitive-limited mechanism while in Ni-BTC MOF and Ni-PEG MOF overall current contribution came from diffusion process indicating the supremacy of diffusion- limited mechanism. Furthermore, for Ni-MOFs synthesized from solvothermal method, diffusion -limited and capacitive-limited processes calculated percentage contributions is shown in **Figure 5.10 (a, b, c, d, e)**. At scan rate (30 mV s^{-1}), the capacitive-limited behavior was evidently prominent in Ni-PM MOF from the current contribution, Ni-BDC MOF and Ni-MEIM MOF nanomaterials because of surface controlled reactions as compared to Ni-BTC MOF and Ni-PEG MOF nanomaterial. The electrode polarization was the reason behind the contribution from closed capacitive observed to lay beyond the CV curves of Ni-BTC and Ni-PEG MOF. However, because of the low capacitance in Ni-BTC MOF and Ni-PEG MOF, the diffusive mechanism accounted for the majority of the charge contribution at high scan rates [118,119].
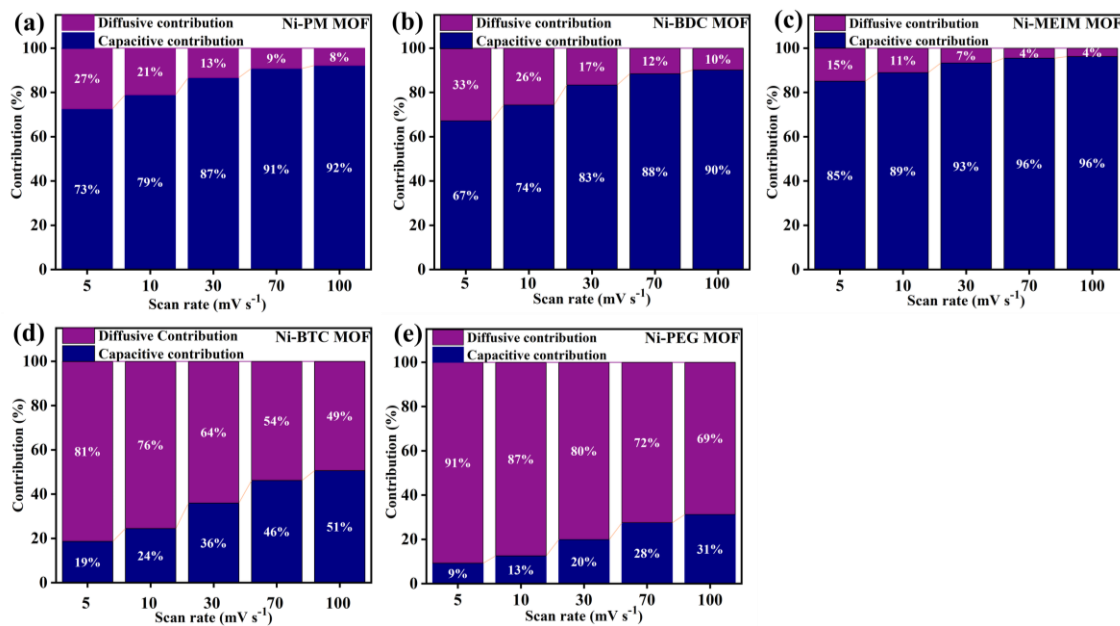
Figure 5. 9 Contribution ratio of Ni-PM MOF (a), Ni-BDC MOF (b), Ni-MEIM MOF (c), Ni-BTC MOF (d) and Ni-PEG MOF (e).
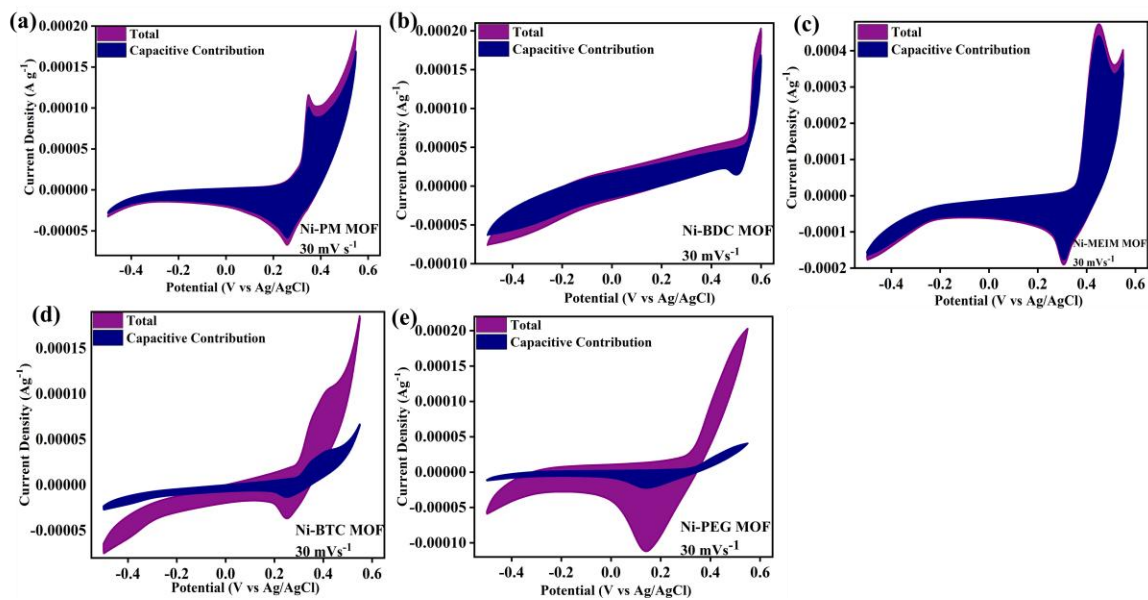
Figure 5. 10 Capacitive current contribution of Ni-PM MOF (a), Ni-BDC MOF (b), Ni- MEIM MOF (c), Ni-BTC MOF (d) and Ni-PEG MOF at 30 mV s^{-1} presented in CV curves.

5.10 Galvanostatic Charge Discharge (GCD) analysis

To examine the prepared Ni-MOFs material's charge/discharge capacity for charge storage and rate analysis, GCD measurements are examined at various current densities. The Ni-MOFs GCD curves in the potential range of -0.5 to 0.55 V are shown in **Figure 5.10 (a, b, c, d, e)**, indicating a good capability rate with current density from 0.5 to 3 A g$^-$^{1}. Ni-MOFs Cs is calculated by using Equation (5.4) from GCD curves; the Cs (specific capacitance) of all prepared electrode material as calculated at corresponding current densities of 0.5, 0.7, 1, 2 and 3 A g^{-1} is shown in **Table 5.3**. The GCD curves of the prepared material's depict the pseudocapacitive behavior. The symmetrical GCD curves of the Ni-MOFs suggest a high degree of electrochemical reversibility, which improves the reaction kinetics [120]. The bar graph represents a comparison of the Cs (specific capacitance) at different current densities of all the prepared electrodes **Figure 5.11(f)**. Equations (5.6) and (5.7) are used to calculate the energy density and power density of prepared Ni-MOFs, which are based on GCD curves at different current densities.

$$C_s = \frac{I \times t}{m \times \Delta V} \qquad\qquad (5.5)$$

Equation (5.5) is used to compute specific capacitance based on the GCD curves.

Equation (5.6) is used to compute the energy density.

$$E_s = \frac{C \times \Delta V^2}{2 \times 3.6} \qquad\qquad (5.6)$$

However, Equation (5.7) is used to calculate power density.

$$P = \frac{E}{\Delta t} \qquad\qquad (5.7)$$
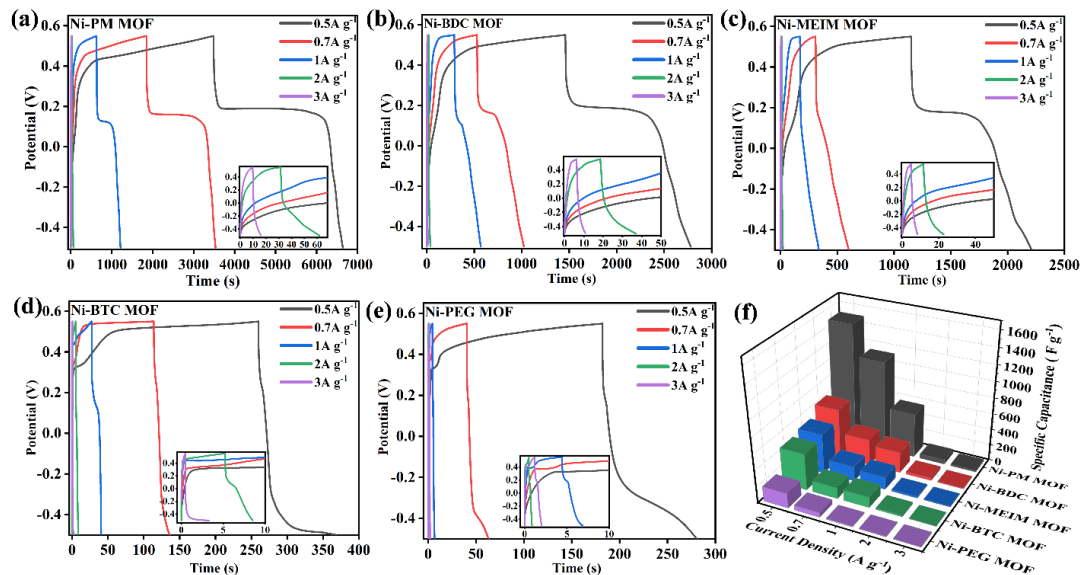
Figure 5. 11 GCD curves of the prepared electrodes at 0.5, 0.7 ,1, 2 and 3 A g^{-1} (a, b, c, d, e), Specific capacitance of prepared electrodes at different current densities calculated from GCD curves (f) and Ragone plot (power density vs energy density) (g).
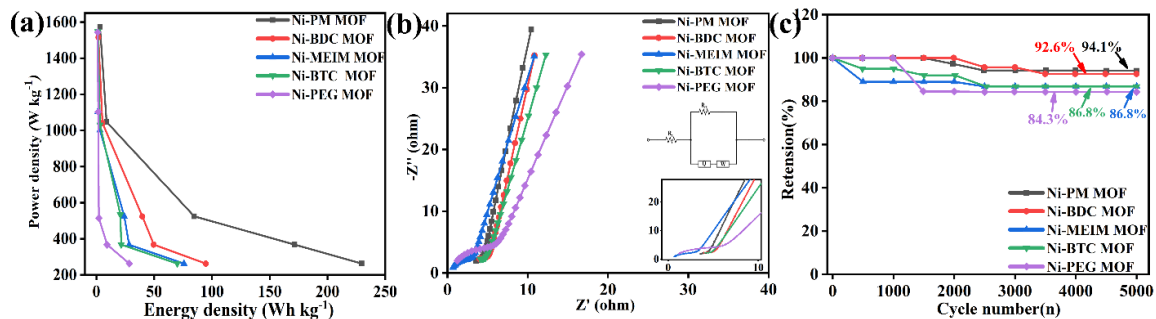
Figure 5. 12 (a) Ragone plot (power density vs energy density) of all Ni-MOFs. (b) Nyquist plot and (c) Cyclic stability of Ni-PM, Ni-BDC, Ni-MEIM, Ni-BTC, and Ni-PEG MOF electrodes after 5000 cycles at 2 A g^{-1}. (c) Cyclic stability of Ni-PM MOF, Ni-BDC MOF, Ni-MEIM MOF, Ni-BTC MOF, and Ni-PEG MOF after 5000 cycles at 2 A g^{-1}

Figure 5.12 (a) shows the Ragone plot of all synthesized MOFs. Equations (8) and (9) are used to calculate the energy density and power density of prepared Ni-MOFs, which are based on GCD curves at different current densities. Among all Ni-PM MOF electrode shows the highest Cs and power density of 263, 368, 524, 1047 and 1575 W kg^{-1} at energy density of 229.6, 172, 84.6, 9, and 3 Wh kg^{-1}.

Table 5. 3 Specific capacitance of prepared Ni-MOFs at 0.5, 0.7, 1, 2 and 3 A g^{-1}

Current Density (A g^{-1})	Specific capacitance (F g^{-1})				
	Ni-PM MOF	Ni-BDC MOF	Ni-MEIM MOF	Ni-BTC MOF	Ni-PEG MOF
0.5	1500	618	495	457	186
0.7	1120	324	185	140	60
1	553	260	157	133	14
2	57	34	21	20	10
3	20	11	11	8	7

Table 5. 4 Values of Rs and Rct determined using Randell's circuit.

Electrode Material	R$_s$ Ω	R$_{ct}$ Ω
Ni-PM MOF	3.56	0.82
Ni-BDC MOF	3.91	1.12
Ni-MEIM MOF	0.68	2.46
Ni-BTC MOF	1.23	3.32
Ni-PEG MOF	1.18	4.48

5.11 EIS analysis

The purpose of EIS was to further explore the prepared electrodes impedance mechanism and charge transfer kinetics. **Figure 5.11(b)** displays their Nyquist plots, which are composed of three parts. The plot's high frequency intercept on the x-axis is known as solution resistance (Rs). The charge transfer resistance (Rct) cumulative contribution is responsible for the semicircle component at high to medium frequency [121].

The Warburg resistance (Rw) is the linear line that indicates the diffusive contribution at the end. With the CHI 660E, EIS data equivalent circuit fitting is done. The corresponding circuit is displayed in **Fig. 11(b)** inset. It helps to explain why Ni-PM MOF has larger Cs. The (Rs) and (Rct) of all the prepared electrodes are demonstrated in **Table 5.4**. Among them Ni-PM MOF electrode has the lowest estimated Rct value 0.82 Ω in 3 M KOH, because of its higher electrochemical surface area (ECSA) and BET, which allow electrons and ions to move more easily and quickly. Since Ni-PM MOF has the lowest Rct in the medium, due to building up of opposing charges on electrode surface causes an electric double layer to develop quickly [122]. It helps to explain why Ni-PM MOF has a larger specific capacitance.

A key performance indicator for supercapacitors is cyclic stability, which shows how well the device sustains its charge/discharge efficiency over several cycles. Throughout their operation, supercapacitors go through numerous cycles of charging and discharging to provide rapid energy bursts. The ability of supercapacitors to sustain high efficiency, dependability, and durability, all essential for their long-term performance and usefulness in a variety of applications requires cyclic stability. Therefore, cyclic stability in 3 M KOH of all the synthesized Ni-MOFs was tested for 5000 cycles at 2 A g^{-1}. The specific capacitance retention rate of 94.1% ,92.6%, 86.8% ,86.8% and 84.3 % is shown by Ni-PM, Ni-BDC, Ni-MEIM, Ni-BTC and Ni-PEG MOF. It indicates that the Electrode materials do not undergo large significant structural changes during charge discharge cycles. The GCD curves stability graph is displayed in **Figure 5.11(c).**

Summary Of Research Work

In summary, we developed a simple, affordable, and scalable solvothermal technique to prepare five distinct Ni-MOFs using five distinct linkers and were successfully prepared using solvothermal method technique. Their application as supercapacitor electrodes were evaluated, and the prepared materials were characterized using a variety of techniques, including FTIR, XRD, SEM, and BET. Ni-PM MOF showed the highest electrochemical performance among all five electrodes exhibiting high Specific capacitance of 1497 F g^{-1} (0.5 A g^{-1}) with cycle life of 94.1% over 5000 runs (2 A g^{-1}). Moreover, Ni-PM MOF delivers power density of 1575 W kg^{-1} (3 A g^{-1}) and Energy density of 229 Wh kg^{-1}(0.5 A g^{-1}). Ni-PM MOF has the least Rct as compared to the other four electrodes. The current study compares each of these MOFs based on their particle size, surface area, electrochemical conductivity, and structure analyzed by characterization. The products can be utilized directly as electrode materials once they are prepared. This work not only offers a crucial concept for producing high-performing Ni-MOFs but also provides a further understanding about their structures and brief comparison of their properties based on different ligands and metal sulfate used.

CHAPTER 6: CONCLUSION AND FUTURE RECOMMENDATION

6.1 Conclusion

In this work, five different Ni-MOFs were synthesized and their electrochemical properties examined as supercapacitor electrode materials. The solvothermal method was utilized to synthesize these samples. The successful synthesis of Ni-MOFs in all prepared electrodes was validated by the XRD data. The SEM analysis revealed a complex network of pores as well as the agglomerated uniform and non-uniform size distribution of particles. Furthermore, Ni-PM MOF showed the highest electrochemical performance among all five electrodes exhibiting high Specific capacitance of 1497 F g^{-1} (0.5 A g^{-1}) with cycle life of 94.1% over 5000 runs (2 A g^{-1}). Moreover, Ni-PM MOF delivers power density of 1575 W kg-1 (3 A g^{-1}) and Energy density of 229 Wh kg^{-1}(0.5 A g^{-1}). Ni-PM MOF has the least Rct as compared to the other four electrodes. Therefore, Ni-PM MOF with remarkable stability and pseudocapacitive properties for supercapacitor can be used as best electrode material. This study demonstrated the simple and economical preparation of Ni-MOFs-derived electrodes for use in high performance supercapacitors offering providing notable energy storage capacity, outstanding cyclic stability, and effective charge-discharge properties. This work showed how to easily and affordably prepare Ni-MOF's derived electrodes for use in high-performance supercapacitors

6.2 Future Recommendation

- ➢ The Ni-PM MOF can be used as an electrode material for batteries as well.
- ➢ Investigate adding or changing the electrolyte composition to increase capacitance and ion mobility, which will improve energy storage performance overall.
- ➢ Adjust operating temperatures to optimize efficiency while considering how temperature affects material performance and electrochemical processes

REFERENCES

[1]   S. Wu, J. Liu, H. Wang, and H. Yan, "A review of performance optimization of MOF-derived metal oxide as electrode materials for supercapacitors," Int J Energy Res, vol. 43, no. 2, pp. 697–716, Feb. 2019, doi: 10.1002/ER.4232.

[2]   Q. Hu et al., "Facile syntheses of perovskite type LaMO3 (M=Fe, Co, Ni) nanofibers for high performance supercapacitor electrodes and lithium-ion battery anodes," J Alloys Compd, vol. 852, Jan. 2021, doi: 10.1016/J.JALLCOM.2020.157002.

[3]   Y. Liu, I. Murtaza, A. Shujia, and H. Meng, "Interfacial modification for heightening the interaction between PEDOT and substrate towards enhanced flexible solid supercapacitor performance," Chemical Engineering Journal, vol. 379, p. 122326, Jan. 2020, doi: 10.1016/J.CEJ.2019.122326.

[4]   Y. P. Gao, Z. B. Zhai, Q. Q. Wang, Z. Q. Hou, and K. J. Huang, "Cycling profile of layered MgAl2O4/reduced graphene oxide composite for asymmetrical supercapacitor," J Colloid Interface Sci, vol. 539, pp. 38–44, Mar. 2019, doi: 10.1016/J.JCIS.2018.12.045.

[5]   Z. Meng et al., "Tailoring NiCoAl layered double hydroxide nanosheets for assembly of high-performance asymmetric supercapacitors," J Colloid Interface Sci, vol. 583, pp. 722–733, Feb. 2021, doi: 10.1016/J.JCIS.2020.08.120.

[6]   S. Shin and M. W. Shin, "Nickel metal–organic framework (Ni-MOF) derived NiO/C@CNF composite for the application of high performance self-standing supercapacitor electrode," Appl Surf Sci, vol. 540, p. 148295, Feb. 2021, doi: 10.1016/J.APSUSC.2020.148295.

[7]   B. Chameh, M. Moradi, S. Hajati, and F. A. Hessari, "Design and construction of ZIF (8 and 67) supported Fe3O4 composite as advanced materials of highperformance supercapacitor," Physica E Low Dimens Syst Nanostruct, vol.126,p.114442,Feb.2021,doi:10.1016/J.PHYSE.2020.1144.

[8]   Y. Du, P. Xiao, J. Yuan, and J. Chen, "Research Progress of Graphene-Based Materials on Flexible Supercapacitors," Coatings 2020, Vol. 10, Page 892, vol. 10, no. 9, p. 892, Sep. 2020, doi: 10.3390/COATINGS10090892.

[9]   Y. P. Gao and K. J. Huang, "NiCo2S4 Materials for Supercapacitor Applications," Chem Asian J, vol. 12, no. 16, pp. 1969–1984, Aug. 2017, doi: 10.1002/ASIA.201700461.

[10] B. Chameh, M. Moradi, S. Hajati, and F. A. Hessari, "Design and construction of ZIF (8 and 67) supported Fe_3O_4 composite as advanced materials of highperformance supercapacitor," Physica E Low Dimens Syst Nanostruct, vol. 126, p. 114442, Feb. 2021, doi: 10.1016/J.PHYSE.2020.114442.

[11] W. Niu et al., "Synthesis of nickel sulfide-supported on porous carbon from a natural seaweed-derived polysaccharide for high-performance supercapacitors," J Alloys Compd, vol. 853, p. 157123, Feb. 2021, doi: 10.1016/J.JALLCOM.2020.157123.

[12] T. Pettong et al., "High-Performance Asymmetric Supercapacitors of $MnCo_2O_4$ Nanofibers and N-Doped Reduced Graphene Oxide Aerogel," ACS Appl Mater Interfaces, vol. 8, no. 49, pp. 34045–34053, Dec. 2016, doi:10.1021/ACSAMI.6B09440/ASSET/IMAGES/AM-2016-09440Z.

[13] L. Sun, Q. Fu, and C. Pan, "Mn_3O_4 embedded 3D multi-heteroatom codoped carbon sheets/carbon foams composites for high-performance flexible supercapacitors," J Alloys Compd, vol. 849, p. 156666, Dec. 2020, doi: 10.1016/J.JALLCOM.2020.156666.

[14] W. Zhou et al., "Polypyrrole doped with dodecyl benzene sulfonate electrodeposited on carbon fibers for flexible capacitors with high-performance," Electrochim Acta, vol. 176, pp. 594–603, Sep. 2015, doi: 10.1016/J.ELECTACTA.2015.07.026.

[15] S. Liu, Q. Feng, C. Zhang, and T. Liu, "Molten salt-confined pyrolysis towards carbon nanotube-backboned microporous carbon for high-energy-density and durable supercapacitor electrodes," Nanotechnology, vol. 32, no. 9, p. 095605, Dec. 2020, doi: 10.1088/1361-6528/ABCBC5.

[16] M. Zhang, Z. Song, H. Liu, A. Wang, and S. Shao, "MoO_2 coated few layers of MoS_2 and FeS_2 nanoflower decorated S-doped graphene inter over lapped network for high-energy asymmetric supercapacitor," J Colloid Interface Sci, vol. 584, pp.418–428, Feb. 2021, doi: 10.1016/J.JCIS.2020.10.005.

[17] P. Wu et al., "A Low-Cost, Self-Standing $NiCo_2O_4$@CNT/CNT Multilayer Electrode for Flexible Asymmetric Solid-State Supercapacitors," Adv Funct Mater, vol. 27, no. 34, p. 1702160, Sep. 2017, doi: 10.1002/ADFM.201702160.

[18] Y. Liu et al., "Structural evolution of porous graphitic carbon nanosheets based on quinonyl decomposition for supercapacitor electrodes," Appl Surf Sci, vol. 537, p. 147824, Jan. 2021, doi: 10.1016/J.APSUSC.2020.147824.

[19] S. Zhai et al., "A novel high performance flexible supercapacitor based on porous carbonized cotton/ZnO nanoparticle/CuS micro-sphere," Colloids Surf APhysicochem Eng Asp, vol. 584, p. 124025, Jan. 2020, doi: 10.1016/J.COLSURFA.2019.124025.

[20] W. He, C. Wang, F. Zhuge, X. Deng, X. Xu, and T. Zhai, "Flexible and high energy density asymmetrical supercapacitors based on core/shell conducting polymer nanowires/manganese dioxide nanoflakes," Nano Energy, vol. 35, pp. 242–250, May 2017, doi: 10.1016/J.NANOEN.2017.03.045.

[21] B. Liu et al., "Optimized synthesis of nitrogen-doped carbon with extremely high surface area for adsorption and supercapacitor," Appl Surf Sci, vol. 538, p. 147961, Feb. 2021, doi: 10.1016/J.APSUSC.2020.147961.

[22] Y. Zhang et al., "Synthesis of faradaic-active N, O-doped carbon nanosheets from m-trihydroxybenzene and piperazine for high-performance supercapacitor," Appl Surf Sci, vol. 538, p. 148040, Feb. 2021, doi: 10.1016/J.APSUSC.2020.148040.

[23] P. Avasthi, N. Arya, M. Singh, and V. Balakrishnan, "Fabrication of iron oxideCNT based flexible asymmetric solid state supercapacitor device with high cyclic stability," Nanotechnology, vol. 31, no. 43, p. 435402, Jul. 2020, doi: 10.1088/13616528/ABA2A0.

[24] G. Yang and S. J. Park, "MnO_2 and biomass-derived 3D porous carbon composites electrodes for high performance supercapacitor applications," J Alloys Compd, vol. 741, pp. 360–367, Apr. 2018, doi: 10.1016/J.JALLCOM.2018.01.108.

[25] C. Li et al., "MnOx nanosheets anchored on a bio-derived porous carbon framework for high-performance asymmetric supercapacitors," Appl Surf Sci, vol. 527, p. 146842, Oct. 2020, doi: 10.1016/J.APSUSC.2020.146842.

[26] N. Wang, P. Zhao, K. Liang, M. Yao, Y. Yang, and W. Hu, "CVD-grown polypyrrole nanofilms on highly mesoporous structure MnO_2 for high performance asymmetric supercapacitors," Chemical Engineering Journal, vol. 307, pp. 105– 112, Jan. 2017, doi: 10.1016/J.CEJ.2016.08.074.

[27] H. Chen, W. Li, M. He, X. Chang, X. Zheng, and Z. Ren, "Vertically oriented carbon nanotube as a stable frame to support the Co0.85Se nanoparticles for high performance supercapacitor electrode," J Alloys Compd, vol. 855, p. 157506, Feb. 2021, doi: 10.1016/J.JALLCOM.2020.157506.

[28] M. Ates and M. Yildirim, "The synthesis of rGO/RuO_2, rGO/PANI, RuO_2/PANI and rGO/RuO_2/PANI nanocomposites and their supercapacitors," Polymer Bulletin, vol. 77, no. 5, pp. 2285–2307, May 2020, doi: 10.1007/S00289-019-028508/TABLES/4.

[29] C. W. Kuo, J. C. Chang, B. W. Wu, and T. Y. Wu, "Electrochemical characterization of RuO_2-Ta_2O_5/polyaniline composites as potential redox electrodes for supercapacitors and hydrogen evolution reaction," Int J Hydrogen Energy, vol. 45, no. 42, pp. 22223–22231, Aug. 2020, doi: 10.1016/J.IJHYDENE.2019.08.059.

[30] H. Ibrahim, A. Ilinca, and J. Perron, "Energy storage systems—Characteristics and comparisons," Renewable and Sustainable Energy Reviews, vol. 12, no. 5, pp. 1221– 1250, Jun. 2008, doi: 10.1016/J.RSER.2007.01.023.

[31] S. Pan, J. Ren, X. Fang, and H. Peng, "Integration: An Effective Strategy to Develop Multifunctional Energy Storage Devices," Adv Energy Mater, vol. 6, no. 4, p. 1501867, Feb. 2016, doi: 10.1002/AENM.201501867.

[32] A. G. Olabi, Q. Abbas, A. Al Makky, and M. A. Abdelkareem, "Supercapacitors as next generation energy storage devices: Properties and applications," Energy, vol. 248, p. 123617, Jun. 2022, doi: 10.1016/J.ENERGY.2022.123617.

[33] X. Ji, "A paradigm of storage batteries," Energy Environ Sci, vol. 12, no. 11, pp. 3203–3224, Nov. 2019, doi: 10.1039/C9EE02356A.

[34] T. H. Nguyen, A. Fraiwan, and S. Choi, "Paper-based batteries: A review," Biosens Bioelectron, vol. 54, pp. 640–649, Apr. 2014, doi: 10.1016/J.BIOS.2013.11.007.

[35] "What is the battery application? -Tycorun Batteries." Accessed: Mar. 23, 2024. [Online]. Available: https://www.tycorun.com/blogs/news/what-is-the-batteryapplication.

[36] H. Qiao and Q. Wei, "Functional nanofibers in lithium-ion batteries," Functional Nanofibers and their Applications, pp. 197–208, 2012, doi: 10.1533/9780857095640.2.197.

[37] T. Kim, W. Song, D. Y. Son, L. K. Ono, and Y. Qi, "Lithium-ion batteries: outlook on present, future, and hybridized technologies," J Mater Chem A Mater, vol. 7, no. 7, pp. 2942–2964, Feb. 2019, doi: 10.1039/C8TA10513H.

[38] B. Scrosati, J. Hassoun, and Y. K. Sun, "Lithium-ion batteries. A look into the future," Energy Environ Sci, vol. 4, no. 9, pp. 3287–3295, Aug. 2011, doi: 10.1039/C1EE01388B.

[39] W. H. Low, P. S. Khiew, S. S. Lim, C. W. Siong, and E. R. Ezeigwe, "Recent development of mixed transition metal oxide and graphene/mixed transition metal oxide-based hybrid nanostructures for advanced supercapacitors," J Alloys Compd, vol. 775, pp. 1324–1356, Feb. 2019, doi: 10.1016/J.JALLCOM.2018.10.102.

[40] M. E. Şahin, F. Blaabjerg, and A. Sang wong wanich, "A Comprehensive Review on Supercapacitor Applications and Developments," Energies 2022, Vol. 15, Page 674, vol. 15, no. 3, p. 674, Jan. 2022, doi: 10.3390/EN15030674.

[41] E. Frackowiak, "Carbon materials for supercapacitor application," Physical Chemistry Chemical Physics, vol. 9, no. 15, pp. 1774–1785, Apr. 2007, doi: 10.1039/B618139M.

[42] S. M. Chen, R. Ramachandran, V. Mani, and R. Saraswathi, "Recent advancements in electrode materials for the high-performance electrochemical supercapacitors: A review," Int J Electrochem Sci, vol. 9, no. 8, pp. 4072–4085, 2014, doi: 10.1016/S1452-3981(23)08076-8.

[43] W. Raza et al., "Recent advancements in supercapacitor technology," Nano Energy, vol. 52, pp. 441–473, Oct. 2018, doi: 10.1016/J.NANOEN.2018.08.013.

[44] Z. S. Iro, C. Subramani, and S. S. Dash, "A Brief Review on Electrode Materials for Supercapacitor," Int J Electrochem Sci, vol. 11, no. 12, pp. 10628–10643, Dec. 2016, doi: 10.20964/2016.12.50.

[45] R. Sudhakar, "Mesoporous Materials for High-Performance Electrochemical Supercapacitors," Mesoporous Materials - Properties and Applications, May 2019, doi: 10.5772/INTECHOPEN.85583.

[46] A. Thirumurugan et al., "Hybrid supercapacitors, formation, and new advances with different electrochemical electrodes based on layered double hydroxides (LDHs), metal–organic framework (MOF) materials, smart supercapacitors," Smart Supercapacitors: Fundamentals, Structures, and Applications, pp. 199–226, Jan. 2022, doi: 10.1016/B978-0-323-90530-5.00032-0.

[47] Y. Shi et al., "SnS$_2$ nanodots decorated on RGO sheets with enhanced pseudocapacitive performance for asymmetric supercapacitors," J Alloys Compd, vol. 853, p. 156903, Feb. 2021, doi: 10.1016/J.JALLCOM.2020.156903.

[48] X. Mu et al., "Construction of Hierarchical CNT/rGO-Supported MnMoO4 Nanosheets on Ni Foam for High-Performance Aqueous Hybrid Supercapacitors," ACS Appl Mater Interfaces, vol. 9, no. 41, pp. 35775–35784, Oct. 2017, doi: 10.1021/ACSAMI.7B09005.

[49] Capacitance control of carbon aerogel electrodes | Request PDF." Accessed:Mar.182024.[Online].Available: https://www.researchgate.net/publication/243301337

[50] Graphene-based materials as supercapacitor electrodes - Journal of Material Chemistry (RSC Publishing)." Accessed: Mar. 18, 2024. [Online]. Available: https://pubs.rsc.org/en/content/articlelanding/2010/jm/c000417

[51] J. Guo et al., "Preparation and Characterization of Nanoporous Activated Carbon Derived from Prawn Shell and Its Application for Removal of Heavy Metal Ions," Materials, vol. 12, no. 2, Jan. 2019, doi: 10.3390/MA12020241.

[52] D. Qu and H. Shi, "Studies of activated carbons used in double-layer capacitors," J Power Sources, vol. 74, no. 1, pp. 99–107, Jul. 1998, doi: 10.1016/S03787753(98)00038-X.

[53] B. V. Malozyomov, V. V. Kukartsev, N. V. Martyushev, V. V. Kondratiev, R. V. Klyuev, and A. I. Karlina, "Improvement of Hybrid Electrode Material Synthesis for Energy Accumulators Based on Carbon Nanotubes and Porous Structures," Micromachines 2023, Vol. 14, Page 1288, vol. 14, no. 7, p. 1288, Jun. 2023, doi: 10.3390/MI14071288.

[54] S. M. Chen, R. Ramachandran, V. Mani, and R. Saraswathi, "Recent advancements in electrode materials for the high-performance electrochemical supercapacitors: A review," Int J Electrochem Sci, vol. 9, no. 8, pp. 4072–4085, 2014, doi: 10.1016/S1452-3981(23)08076-8.

[55] M. Mastragostino, C. Arbizzani, and F. Soavi, "Conducting polymers as electrode materials in supercapacitors," Solid State Ion, vol. 148, no. 3–4, pp. 493–498, Jun. 2002, doi: 10.1016/S0167-2738(02)00093-0.

[56] H. Mi, X. Zhang, S. Yang, X. Ye, and J. Luo, "Polyaniline nanofibers as the electrode material for supercapacitors," Mater Chem Phys, vol. 112, no. 1, pp.127– 131, Nov. 2008,doi: 10.1016/J.MATCHEMPHYS.2008.05.022.

[57] J. Qin, C. Li, W. Lu, and H. Zheng, "Fabrication of Poly (3, 4ethylenedioxythiophene)/O−S Co-Doped Porous Carbon Composites as Electrode Materials for Supercapacitors," ChemistrySelect, vol. 7, no. 48, p. e202203840, Dec. 2022, doi: 10.1002/SLCT.202203840.

[58] R. B. Choudhary, S. Ansari, and B. Purty, "Robust electrochemical performance of polypyrrole (PPy) and polyindole (PIn) based hybrid electrode materials for supercapacitor application: A review," J Energy Storage, vol. 29, p. 101302, Jun. 2020, doi: 10.1016/J.EST.2020.101302.

[59] M. Al Zoubi, R. Al-Salman, Y. Li, and F. Endres, "Highly ordered 3D-macroporous poly(para-phenylene) films made by electro polymerization of benzene in an ionic liquid," Zeitschrift fur Physikalische Chemie, vol. 225,no.4,pp.393–403,Apr.2011,doi: 10.1524/ZPCH.2011.0091/MACHINEREADABLECITATION/RIS.

[60] A. Laforgue, P. Simon, C. Sarrazin, and J. F. Fauvarque, "Polythiophene-based supercapacitors," J Power Sources, vol. 80, no. 1–2, pp. 142–148, Jul. 1999, doi: 10.1016/S0378-7753(98)00258-4.

[61] S. Banerjee and K. K. Kar, "Conducting polymers as electrode materials for supercapacitors," Springer Series in Materials Science, vol. 302, pp. 333–352, 2020, doi: 10.1007/978-3-030-52359-6_13/COVER.

[62] M. Manuraj, J. Chacko, K. N. Narayanan Unni, and R. B. Rakhi, "Heterostructure MoS2-RuO2 nanocomposite: A promising electrode material for supercapacitors," J Alloys Compd, vol. 836, p. 155420, Sep. 2020, doi: 10.1016/J.JALLCOM.2020.155420.

[63] H. Xiao, F. Qu, and X. Wu, "Ultrathin NiO nanoflakes electrode materials for supercapacitors," Appl Surf Sci, vol. 360, pp. 8–13, Jan. 2016, doi: 10.1016/J.APSUSC.2015.10.171.

[64] S. Nagamuthu, S. Vijayakumar, and G. Muralidharan, "Synthesis of Mn_3O_4/amorphous carbon nanoparticles as electrode material for high performance supercapacitor applications," Energy and Fuels, vol. 27, no. 6, pp.3508–3515,Jun.2013,doi: 10.1021/EF400212B.

[65] A. Ray et al., "Electrochemical properties of TiO_2-V_2O_5 nanocomposites as a high- performance supercapacitors electrode material," Appl Surf Sci, vol. 443, pp. 581– 591, Jun. 2018, doi: 10.1016/J.APSUSC.2018.02.277.

[66] A. Ramadoss and S. J. Kim, "Improved activity of a graphene–TiO_2 hybrid electrode in an electrochemical supercapacitor," Carbon N Y, vol. 63, pp. 434–445, Nov. 2013, doi: 10.1016/J.CARBON.2013.07.006.

[67] C. C. Raj and R. Prasanth, "Review—Advent of TiO 2 Nanotubes as Supercapacitor Electrode," J Electrochem Soc, vol. 165, no. 9, pp. E345–E358, Jun. 2018, doi: 10.1149/2.0561809JES/XML.

[68] P. Pazhamalai, K. Krishnamoorthy, V. K. Mariappan, and S. J. Kim, "Blue TiO2 nanosheets as a high-performance electrode material for supercapacitors," J Colloid Interface Sci, vol. 536, pp. 62–70, Feb. 2019, doi: 10.1016/J.JCIS.2018.10.031.

[69] Q. Wang, L. Jiao, H. Du, Y. Wang, and H. Yuan, "Fe3O4 nanoparticles grown on graphene as advanced electrode materials for supercapacitors," J Power Sources, vol. 245, pp. 101–106, Jan. 2014, doi: 10.1016/J.JPOWSOUR.2013.06.035.

[70] X. Wang, A. Hu, C. Meng, C. Wu, S. Yang, and X. Hong, "Recent Advance in Co_3O_4 and Co_3O_4-Containing Electrode Materials for High-Performance Supercapacitors," Molecules 2020, Vol. 25, Page 269, vol. 25, no. 2, p. 269, Jan. 2020, doi: 10.3390/MOLECULES25020269.

[71] A. G. Temam et al., "Recent progress on V2O5 based electroactive materials: Synthesis, properties, and supercapacitor application," Curr OpinElectrochem,vol.38,p.101239,Apr.2023,doi: 10.1016/J.COELEC.2023.101239.

[72] Y. Niu, H. Su, X. Li, J. Li, and Y. Qi, "Synthesis of porous α-MoO_3 microspheres as electrode materials for supercapacitors," J Alloys Compd, vol. 898, p. 162863, Mar. 2022, doi: 10.1016/J.JALLCOM.2021.162863.

[73] Y. Zhang et al., "Electrochemical investigation of MnO_2 electrode material for supercapacitors," Int J Hydrogen Energy, vol. 36, no. 18, pp. 11760–11766, Sep. 2011, doi: 10.1016/J.IJHYDENE.2011.06.020.

[74] S. Korkmaz, F. Meydaneri Tezel, and A. Kariper, "Synthesis and characterization of GO/IrO_2 thin film supercapacitor," J Alloys Compd, vol. 754, pp. 14–25, Jul. 2018, doi: 10.1016/J.JALLCOM.2018.04.170.

[75] J. N. Udeh, R. M. Obodo, A. C. Nkele, A. C. Nwanya, P. M. Ejikeme, and F. I. Ezema, "Recent Advances in Usage of Cobalt Oxide Nanomaterials as

Electrode Material for Supercapacitors," Electrode Materials for Energy Storage and Conversion, pp. 141–170, Nov. 2021, doi: 10.1201/9781003145585-7.

[76] R. Thangappan, R. Dhinesh Kumar, and R. Jayavel, "Synthesis, structural and electrochemical properties of Mn-MoO$_4$/graphene nanocomposite electrode material with improved performance for supercapacitor application," J Energy Storage, vol. 27, p. 101069, Feb. 2020, doi: 10.1016/J.EST.2019.101069.

[77] R. Liang et al., "Transition Metal Oxide Electrode Materials for Supercapacitors: A Review of Recent Developments," Nanomaterials 2021, Vol. 11, Page 1248, vol. 11, no. 5, p. 1248, May 2021, doi: 10.3390/NANO11051248.

[78] C. Yuan, H. Bin Wu, Y. Xie, and X. W. Lou, "Mixed transition-metal oxides: design, synthesis, and energy-related applications," Angew Chem Int Ed Engl, vol. 53, no. 6, pp. 1488–1504, Feb. 2014, doi: 10.1002/ANIE.201303971.

[79] C. Cheng et al., "Self-template synthesis of hollow ellipsoid Ni-Mn sulfides for supercapacitors, electrocatalytic oxidation of glucose and water treatment," Dalton Transactions, vol. 46, no. 16, pp. 5406–5413, 2017, doi: 10.1039/C7DT00355B.

[80] P. Sharma and V. Kumar, "Study of electrode and electrolyte material of supercapacitor," Mater Today Proc, vol. 33, pp. 1573–1578, Jan. 2020, doi: 10.1016/J.MATPR.2020.04.694.

[81] Y. Wang, Y. Lei, J. Li, L. Gu, H. Yuan, and D. Xiao, "Synthesis of 3D-nanonet hollow structured Co$_3$O$_4$ for high-capacity supercapacitor," ACS Appl Mater Interfaces, vol. 6, no. 9, pp. 6739–6747, May 2014, doi: 10.1021/AM500464N/SUPPL_FILE/AM500464N_SI_001.PDF.

[82] H. Y. Lee and J. B. Goodenough, "Supercapacitor Behavior with KCl Electrolyte," J Solid State Chem, vol. 144, no. 1, pp. 220–223, Apr. 1999, doi: 10.1006/JSSC.1998.8128.

[83] S. Sharma and P. Chand, "Supercapacitor and electrochemical techniques: A brief review," Results Chem, vol. 5, p. 100885, Jan. 2023, doi: 10.1016/J.RECHEM.2023.100885.

[84] R. Farma et al., "Physical and Electrochemical Properties of Supercapacitor Electrodes Derived from Carbon Nanotube and Biomass Carbon," Int. J. Electrochem. Sci, vol. 8, pp. 257–273, 2013, Accessed: Mar. 19, 2024. [Online]. Available: www.electrochemsci.org

[85] M. M. Baig, I. H. Gul, S. M. Baig, and F. Shahzad, "The complementary advanced characterization and electrochemical techniques for electrode materials for supercapacitors," J Energy Storage, vol. 44, p. 103370, Dec. 2021, doi: 10.1016/J.EST.2021.103370.

[86]   B. Padha, S. Verma, P. Mahajan, V. Gupta, A. Khosla, and S. Arya, "Role of Electrochemical Techniques for Photovoltaic and Supercapacitor Applications," Crit Rev Anal Chem, 2022, doi: 10.1080/10408347.2022.2096401.

[87]   S. K. Godlaveeti, S. Jangiti, A. R. Somala, H. Maseed, and R. R. Nagireddy, "Different Phase and Morphology Effect of Manganese Oxide on Electrochemical Performance for Supercapacitor Application," J Clust Sci, vol. 32, no. 3, pp. 703– 710, May 2021, doi: 10.1007/S10876-020-01833-4/FIGURES/7.

[88]   K. Seevakan, A. Manikandan, P. Devendran, Y. Slimani, A. Baykal, and T. Alagesan, "Structural, magnetic and electrochemical characterizations of Bi2Mo2O9 nanoparticle for supercapacitor application," J Magn Magn Mater, vol. 486, p. 165254, Sep. 2019, doi: 10.1016/J.JMMM.2019.165254.

[89]   T. Ramesh, R. Vedarajan, N. Rajalakshmi, and L. R. G. Reddy, "Dynamic electrochemical impedance spectroscopy as a rapid screening tool for supercapacitor electrode materials," Journal of Materials Science: Materials in Electronics, vol. 31, no. 2, pp. 1681–1690, Jan. 2020, doi: 10.1007/S10854-019-02686Y/TABLES/2.

[90]   A. Oz, Shany Hershkovitz, Y. Tsur, and S. Hershkovitz, "Electrochemical impedance spectroscopy of supercapacitors: A novel analysis approach using evolutionary programming," AIP Conf Proc, vol. 1627, no. 1, pp. 76–80, Nov. 2014, doi: 10.1063/1.4901661.

[91]   Zhang, C., et al., Preparation and application of Co3O4-Ni-MOF/MWCNTs hybrid for supercapacitor. Ionics, 2021. 27(8): p. 3543-3551.

[92]   Xiao, G., et al., Imidazolate Framework (Zn-Ni (MeIm) 2) Nanohybrids as Electrodes for Supercapacitor Applications. International Journal of Electrochemical Science, 2020. 15(8): p. 8277-8283.

[93]   Xiao, G., et al., Imidazolate Framework (Zn-Ni (MeIm) 2) Nanohybrids as Electrodes for Supercapacitor Applications. International Journal of Electrochemical Science, 2020. 15(8): p. 8277-8283.

[94]   Paul, A., et al., Gold-nanoparticle-encapsulated ZIF-8 for a mediator-free enzymatic glucose sensor by amperometry. ACS Applied Nano Materials, 2018. 1(7): p. 3600-3607.

[95]   Wu, X., et al., Microwave synthesis and characterization of MOF-74 (M= Ni, Mg) for gas separation. Microporous and mesoporous materials, 2013. 180: p. 114-122.

[96]   Díaz-García, M., et al., Nanoscaled M-MOF-74 materials prepared at room temperature. Crystal growth & design, 2014. 14(5): p. 2479-2487.

[97]   Wang, Y., Y. He, and M. Zhou, Fabrication of hierarchical Co (OH) 2@ Ni (OH) 2 core-shell nanosheets on carbon cloth as an advanced electrocatalyst for oxygen evolution reaction. Applied Surface Science, 2019. **479**: p. 1270-1276.

[98]   Liu, L., et al., Facile preparation of novel dandelion-like Fe-doped NiCo2O4 microspheres@ nanomeshes for excellent capacitive property in asymmetric supercapacitors. Journal of Power Sources, 2016. **327**: p. 135-144.

[99]   Xia, P., et al., Hierarchical NiCo2O4@ Ni (OH) 2 core-shell nanoarrays as advanced electrodes for asymmetric supercapacitors with high energy density. Journal of Alloys and Compounds, 2019. **771**: p. 784-792.

[100]   Acharya, J., et al., Leaf-like integrated hierarchical NiCo2O4 nanorods@ Ni-Co-LDH nanosheets electrodes for high-rate asymmetric supercapacitors. Journal of Alloys and Compounds, 2021. **884**: p. 161165.

[101]   Dang, Y., et al., Low-crystalline mixed Fe-Co-MOFs for efficient oxygen evolution electrocatalysis. Journal of Materials Science, 2020. **55**: p. 13951-13963.

[102]   Briggs, D. and G. Beamson, XPS studies of the oxygen 1s and 2s levels in a wide range of functional polymers. Analytical chemistry, 1993. **65**(11): p. 1517-1523.

[103]   Ai, L., et al., Cobalt/cerium-based metal-organic framework composites for enhanced oxygen evolution electrocatalysis. International Journal of Hydrogen Energy, 2022. **47**(26): p. 12893-12902.

[104]   Mathew, S., et al., One-pot synthesis of sustainable carbon dots for analytical and cytotoxicity studies. Biomass Conversion and Biorefinery, 2024. **14**(14): p. 16473-16486.

[105]   Guo, X., Z. Fan, and Z. Jin, Cobalt nanoparticles encapsulated in hollow carbon nitride nanotubes for efficient photocatalytic hydrogen evolution. Energy Technology, 2021. **9**(9): p. 2100499.

[106]   Ge, M., et al., Enhanced photocatalytic degradation performance of antibiotics using magadiite-supported carbon nitride under visible light irradiation. Journal of Inorganic and Organometallic Polymers and Materials, 2022: p. 1-9.

[107]   Zeraati, M., et al., A new nickel metal organic framework (Ni-MOF) porous nanostructure as a potential novel electrochemical sensor for detecting glucose. Journal of Porous Materials, 2022: p. 1-11.

[108]   Sahu, M., et al., Fabrication of Cu2ZnSnS4 light absorber using a cost-effective mechanochemical method for photovoltaic applications. Materials, 2022. **15**(5): p. 1708.

[109] Arul, P. and S.A. John, Size controlled synthesis of Ni-MOF using polyvinylpyrrolidone: new electrode material for the trace level determination of nitrobenzene. Journal of Electroanalytical Chemistry, 2018. **829**: p. 168-176.

[110] Raje, P.G., et al., Exploring the role of metal concentrations on the chemically synthesized Ni-MOFs nanostructures for asymmetric supercapacitor. Journal of Energy Storage, 2024. **95**: p. 112617.

[111] Tan, K. and Y.J. Chabal, Interaction of small molecules within metal organic frameworks studied by in situ vibrational spectroscopy. Metal-organic frameworks, 2016: p. 19-36.

[112] Tan, K. and Y.J. Chabal, Interaction of small molecules within metal organic frameworks studied by in situ vibrational spectroscopy. Metal-organic frameworks, 2016: p. 19-36.

[113] Otun, K.O., et al., Double linker MOF-derived NiO and NiO/Ni supercapacitor electrodes for enhanced energy storage. Colloids and Surfaces A: Physicochemical and Engineering Aspects, 2022. **634**: p. 128019.

[114] Sandford, C., et al., A synthetic chemist's guide to electroanalytical tools for studying reaction mechanisms. Chemical science, 2019. **10**(26): p. 6404-6422.

[115] Dhelipan, M., et al., Activated carbon from orange peels as supercapacitor electrode and catalyst support for oxygen reduction reaction in proton exchange membrane fuel cell. Journal of Saudi Chemical Society, 2017. **21**(4): p. 487-494.

[116] Zheng, S.Q., et al., Solvothermal synthesis of nanostructured nickel-based metal–organic frameworks (Ni-MOFs) with enhanced electrochemical performance for symmetric supercapacitors. Journal of Materials Science, 2023. **58**(29): p. 11894-11913.

[117] Gao, G., et al., Atomic-scale engineering of MOF array confined Au nanoclusters for enhanced heterogeneous catalysis. Nanoscale, 2019. 11(3): p. 1169-1176.

[118] Zheng, J., et al., Shaping of ultrahigh-loading MOF pellet with a strongly anti-tearing binder for gas separation and storage. Chemical Engineering Journal, 2018. 354: p. 1075-1082.

[119] Zhang, X., et al., From rational design of a new bimetallic MOF family with tunable linkers to OER catalysts. Journal of Materials Chemistry A, 2019. 7(4): p. 1616-1628.

[120] Yan, B., Photofunctional MOF-based hybrid materials for the chemical sensing of biomarkers. Journal of Materials Chemistry C, 2019. 7(27): p. 8155-8175.

[121] Zhao, W., et al., MOF derived Ni-Co-S nanosheets on electrochemically activated carbon cloth via an etching/ion exchange method for wearable hybrid supercapacitors. Chemical Engineering Journal, 2019. 371: p. 461-469.

[122] Guo, X., Z. Fan, and Z. Jin, Cobalt nanoparticles encapsulated in hollow carbon nitride nanotubes for efficient photocatalytic hydrogen evolution. Energy Technology, 2021. 9(9): p. 2100499.

LIST OF PUBLICATIONS

1   *ACS Applied Materials & Interfaces*

Synthesis of Ni based metal organic frameworks using five distinct precursors and their energy storage performance as electrodes in supercapacitor

Manuscript ID: am-2024-20722m
Status: Under Review
Submitted on 26 November 2024